Physica D 64 (1993) 185–214
North-Holland

PHYSICA D

Statistical properties of highly excited quantum eigenstates of a strongly chaotic system*

R. Aurich and F. Steiner

II. Institut für Theoretische Physik, Universität Hamburg, Luruper Chaussee 149, W-2000 Hamburg 50, Germany

Received 17 July 1992
Accepted 12 October 1992
Communicated by F.H. Busse

Statistical properties of highly excited quantal eigenstates are studied for the free motion (geodesic flow) on a compact surface of constant negative curvature (hyperbolic octagon) which represents a strongly chaotic system (K-system). The eigenstates are expanded in a circular-wave basis, and it turns out that the expansion coefficients behave as Gaussian pseudo-random numbers. It is shown that this property leads to a Gaussian amplitude distribution $P(\Psi)$ in the semiclassical limit, i.e. the wave-functions behave as Gaussian random functions. This behaviour, which should hold for chaotic systems in general, is nicely confirmed for eigenstates lying 10 000 states above the ground state thus probing the semiclassical limit. In addition, the autocorrelation function and the path-correlation function are calculated and compared with a crude semiclassical Bessel-function approximation. Agreement with the semiclassical prediction is only found, if a local averaging is performed over roughly 1000 de Broglie wavelengths. On smaller scales, the eigenstates show much more structure than predicted by the first semiclassical approximation.

1. Introduction

Until recently, the studies of the quantum mechanical counterparts of classically strongly chaotic systems have mainly concentrated on the properties of the quantal energy spectra leading to the important result that the short-range correlations observed in the quantal energy sequences are in accordance with the universal predictions of random-matrix theory (RMT) [1]. (For recent reviews, see refs. [2–5], and for the particular model studied in this paper, see ref. [6]). While these investigations were therefore devoted to the collective behaviour of many states, one can search, on the other hand, for the fingerprints of classical chaos in a single quantum eigenstate leading to the study of wavefunctions $\Psi(q)$ as well as of the corresponding Wigner functions $W(q, p)$ [7] describing the eigenstates in phase space.

One important question is whether the eigenstates of classically chaotic systems are localized or not. Here a state is called localized if the expansion coefficients with respect to a "generic" basis are large only for a small number of adjacent basis functions and decrease exponentially with increasing distance from the dominant region. The unsatisfactory point is the basis-dependent description and the fact that it is not obvious if a considered basis is actually a generic one. The absence of localization in eigenstates leads to wavefunctions whose statistical properties can be described by RMT [8], as numerical studies show in the case of kicked tops [9]. Different localized eigenstates having no overlap with respect to such a generic basis have no reason to generate correlations among their quantal energies and thus do not obey the pre-

*Supported by Deutsche Forschungsgemeinschaft under Contract No. DFG-Ste 241/4-3.

dictions of RMT. The dependence of the statistical properties of the quantal energy spectra on the localization is well studied for the kicked rotator and for the kicked top (for a review, see refs. [10] and [5], respectively).

Another important question is whether the wavefunctions $\Psi(q)$ possess so-called "scars" [11], i.e. regions in the neighbourhood of the classical periodic orbits where the intensity $|\Psi(q)|^2$ differs significantly from the statistically expected mean. The discussion of scars has been preceded by the "semiclassical eigenfunction hypothesis" [12–14] which states that the Wigner function semiclassically condenses like a δ-function on the energy surface in analogy to the classical Liouville density

$$W(q, p) \sim \delta(H(q, p) - E) . \tag{1}$$

This is the expected classical limit for $\hbar = 0$ which differs, however, from the semiclassical behaviour, where $\hbar$ is small but not zero. It is worthwhile to note that a similar result has been obtained in the semiclassical limit by Zelditch [15] and Colin de Verdière [16] for the free motion on compact Riemann surfaces, i.e. exactly the systems to be studied in this paper. After Heller's discovery of scars in the stadium billiard [11], the semiclassical eigenfunction hypothesis has been modified to incorporate the contributions from the classical orbits which add oscillatory contributions to the smooth background (1)

$$W(q, p) \sim \delta(H(q, p) - E) + \sum_j W^j_{\text{scar}}(q, p) . \tag{2}$$

Here j labels all periodic orbits (including repetitions) with energy E. The semiclassical scar-contribution was worked out by Bogomolny [17] and by Berry [18]. For the systems which we shall discuss in this paper, we have derived an *exact* orbit theory in [19], where it is shown how the exact theory can be approximated to yield Bogomolny's semiclassical theory. (Note that the original version of the scar theory refers not to single eigenstates, but to averages over groups of states. If, however, a suitable smoothing is considered as in ref. [19], it is possible to single out a given eigenstate). Indeed, this theory seems to predict an increased intensity of the wavefunction and the Wigner function in the neighbourhood of periodic orbits. However, in the semiclassical limit $\hbar \to 0$, each periodic-orbit contribution, being of higher order in $\hbar$, shrinks to zero, and only their collective behaviour describes the eigenstate. Up to now it is unclear how the contributions of a single short periodic orbit can survive in the semiclassical limit and whether all scars are in a genuine connection with a single periodic orbit, or if they are merely a product of a random process. The question of scars in the strongly chaotic systems, which we study in this paper, will be discussed in a forthcoming paper. Here we are mainly interested in the statistical properties of the wavefunctions.

In this paper we study a conservative Hamiltonian system which classically consists of a point particle sliding freely on a closed surface of constant negative curvature. One is led to study such a system because it can be viewed as a simple case of a large class of general potential problems. In general, the motion of a particle which is solely determined by a given potential $V(q)$ can be considered in Jacobian coordinates as the geodesic motion on a curved manifold, where the curvature is determined by the potential $V(q)$. Since Gelfand and Fomin showed that negative curvature is necessary for a system to be chaotic [20], it is natural to study the simplest case, i.e. the case of constant negative Gaussian curvature $K = -1$. For more details on the physical significance of this model which is one of the main testing grounds of our ideas about quantum chaos, we refer to our earlier paper [6].

The surfaces to be considered are compact Riemann surfaces $\mathcal{F}$ of constant negative curvature $K = -1$ with genus $g = 2$, i.e. they have the topology of a sphere with two handles. Due to the Gauss–Bonnet theorem, $\text{Area}(\mathcal{F}) = 4\pi(g - 1)$, the area of such a surface is $\text{Area}(\mathcal{F}) = 4\pi$.

The sphere with two handles can be cut so that one obtains an octagon with geodesic edges, where opposite sides must be identified which leads to periodic boundary conditions. A given octagon is mapped into the Poincaré disc $\mathcal{D}$, which consists of the interior of the unit circle in the complex z-plane ($z = x_1 + \mathrm{i}x_2$) endowed with the hyperbolic metric

$$g_{ij} = \frac{4}{(1 - x_1^2 - x_2^2)^2}\,\delta_{ij}\,, \quad i, j = 1, 2\,, \tag{3}$$

corresponding to constant negative Gaussian curvature $K = -1$. (This fixes the length scale.) The classical motion is determined by the Hamiltonian $H = (1/2m)p_i g^{ij} p_j$, $p_i = m g_{ij}\,\mathrm{d}x^j/\mathrm{d}t$, and the geodesics are circles intersecting the boundary of the Poincaré disc $\mathcal{D}$ perpendicularly.

The quantum mechanical system is governed by the Schrödinger equation

$$-\Delta\Psi_n(z) = E_n\,\Psi_n(z)\,,$$
$$\text{with } \Delta = \tfrac{1}{4}(1 - x_1^2 - x_2^2)^2\left(\frac{\partial^2}{\partial x_1^2} + \frac{\partial^2}{\partial x_2^2}\right), \tag{4}$$

where we used $\hbar = 2m = 1$. The periodic boundary conditions are realized by identifying the points z and $z' \equiv b(z)$,

$$b(z) := \frac{\alpha z + \beta}{\beta^* z + \alpha^*}\,,$$
$$|\alpha|^2 - |\beta|^2 = 1\,, \tag{5}$$

where the "boosts"

$$b = \begin{pmatrix} \alpha & \beta \\ \beta^* & \alpha^* \end{pmatrix} \in \mathrm{SU}(1,1)/\{\pm\mathbf{1}\}$$

are chosen such that they map a given edge onto the opposite edge. Four boosts are sufficient for the description of a given octagon. These four boosts and their inverses are the generators of the Fuchsian group Γ which tessellates the Poincaré disc $\mathcal{D}$. The solutions of the Schrödinger equation (4) have to obey the periodic boundary conditions

$$\Psi(z) = \Psi(b(z)) \quad \text{for all } b \in \Gamma\,, \tag{6}$$

and are normalized according to

$$\int\!\!\int_{\mathcal{F}} \mathrm{d}x_1\,\mathrm{d}x_2\,\frac{4}{(1 - x_1^2 - x_2^2)^2}\,\Psi_m^*(z)\,\Psi_n(z) = \delta_{mn}\,. \tag{7}$$

For more details of this model, see the well-written introductions in refs. [4,21] and our earlier papers [6,19,22].

2. Computation of highly excited states

In our earlier studies on the wavefunctions [19] and quantal energies [6,22] of hyperbolic octagons, the computations have been based on the finite-element method. This method relies on a variational principle and thus yields upper bounds for the quantal energies. By using an algorithm with a high order of convergence, we were able to compute the first 200 eigenvalues of a given asymmetric hyperbolic octagon with sufficient accuracy. But to proceed to much higher excited levels, the finite-element method is not suited. The method outlined below uses instead the "direct boundary-element method", which requires the computation of a determinant of an energy-dependent matrix whose zeros, or in practical applications, whose minima yield the desired quantal energies. Whereas the finite-element method yields all the first n quantal energies after solving the eigenvalue problem at once, the boundary-element method forces one to compute many determinants to locate a single eigenvalue. The advantage of the latter is that, on the one hand, it does not rely on a variational principle, and, on the other hand, it reduces the dimension of the problem by one, because the unknown wavefunction has only to be computed on the boundary of the octagon instead on the whole fundamental domain $\mathcal{F}$. It turns out that these facts enable us to compute even the

20 000th excited level of a general asymmetric octagon.

To derive the basic integral equation for our problem, we rewrite the Schrödinger equation (4) as

$$\left[\boldsymbol{\nabla}\cdot\boldsymbol{\nabla} + \frac{4}{(1-|z|^2)^2}\, E\right]\Psi(z) = 0$$

$$\text{with } \boldsymbol{\nabla} := \left(\frac{\partial}{\partial x_1}, \frac{\partial}{\partial x_2}\right). \tag{8}$$

Let $u(z)$ and $v(z)$ be normalizable functions on the fundamental domain $\mathcal{F}$, then the following integral can be cast by Green's theorem into an integral over the boundary $\partial\mathcal{F}$ of the fundamental domain $\mathcal{F}$:

$$\int_{\mathcal{F}} \mathrm{d}z' \left[v(z') \left(\boldsymbol{\nabla}'\cdot\boldsymbol{\nabla}' + \frac{4}{(1-|z'|^2)^2}\, E\right) u(z') - u(z') \left(\boldsymbol{\nabla}'\cdot\boldsymbol{\nabla}' + \frac{4}{(1-|z'|^2)^2}\, E\right) v(z') \right]$$

$$= \int_{\partial\mathcal{F}} \mathrm{d}\gamma_{z'} \left(v(z') \frac{\partial u(z')}{\partial n_{z'}} - u(z') \frac{\partial v(z')}{\partial n_{z'}} \right). \tag{9}$$

Here the integration is with respect to the Euclidean measure, and it is worthwhile to remark that the terms due to the hyperbolic metric cancel in the first line ($\mathrm{d}z' = \mathrm{d}x_1' \,\mathrm{d}x_2'$). $\partial/\partial n_{z'}$ is the normal derivative with respect to the boundary $\partial\mathcal{F}$ at the boundary point z', and $\mathrm{d}\gamma_{z'}$ is the line-element on $\partial\mathcal{F}$. Now we set $v(z')$ equal to a solution $\Psi(z')$ of the Schrödinger equation (4) and $u(z')$ equal to the free Green's function $G_0(z, z', E)$ on the Poincaré disc defined by

$$\left(\boldsymbol{\nabla}\cdot\boldsymbol{\nabla} + \frac{4}{(1-|z|^2)^2}\, E\right) G_0(z, z', E) = \delta(z - z'). \tag{10}$$

Then one obtains from (9) the basic integral equation

$$\int_{\partial\mathcal{F}} \left(\Psi(z') \frac{\partial G_0(z, z', E)}{\partial n_{z'}} - G_0(z, z', E) \frac{\partial \Psi(z')}{\partial n_{z'}} \right) \mathrm{d}\gamma_{z'}$$

$$= \int_{\mathcal{F}} \mathrm{d}z'\, \Psi(z')\, \delta(z - z')$$

$$= \begin{cases} \Psi(z), & z \in \mathcal{F} \text{ but } z \notin \partial\mathcal{F} \\ \frac{1}{2}\Psi(z), & z \in \partial\mathcal{F} \\ 0, & \text{otherwise}. \end{cases} \tag{11}$$

The Green's function of eq. (10) is known to be proportional to the Legendre function of the second kind $Q_\nu(x)$ with $x > 1$ (see, e.g. refs. [21,23]):

$$G_0(z, z', E) = \frac{1}{2\pi}\, Q_{-\frac{1}{2}-ip}(\cosh d(z, z')), \tag{12}$$

where $E = \frac{1}{4} + p^2$, and

$$\cosh d(z, z') := 1 + \frac{2|z - z'|^2}{(1-|z|^2)(1-|z'|^2)} \tag{13}$$

defines the hyperbolic distance $\tau \equiv d(z, z')$ between z and z'.

The efficiency of a numerical application of eq. (11) depends heavily on an effective algorithm for the accurate computation of $Q_\nu(x)$. Fast converging series can be obtained from the following relation of $Q_\nu(x)$ to the hypergeometric function (see p. 153 in ref. [24])

$$Q_\nu(x) = \frac{\sqrt{\pi}}{(2x)^{\nu+1}} \frac{\Gamma(\nu+1)}{\Gamma(\nu+\frac{3}{2})} \times {}_2F_1\left(\frac{\nu}{2}+1, \frac{\nu}{2}+\frac{1}{2}; \nu+\frac{3}{2}; \frac{1}{x^2}\right), \quad |x| > 1. \tag{14}$$

From (14) one gets for $\cosh\tau > 1$

$$Q_{-\frac{1}{2}-ip}(\cosh\tau) = \sqrt{\pi}(2\cosh\tau)^{-\frac{1}{2}+ip}\sum_{k=0}^{\infty}\frac{a_k}{\cosh^{2k}\tau}, \tag{15}$$

where the coefficients a_k are determined by the recursion formula

$$a_k = \frac{1-E+2ip(1-2k)+4k(k-1)}{4k(k-ip)}\,a_{k-1}$$

$$\text{with } a_0 = \frac{\Gamma(\frac{1}{2}-ip)}{\Gamma(1-ip)}. \tag{16}$$

This yields a fast converging series for $\tau \gg 0$. In the opposite limit $\tau \to 0$, the Green's function has a logarithmic divergence, being analogous to the short-distance singularity of the Green's function for Euclidean billiards. It is thus desirable to use an expression which gives the corrections to the logarithmic divergence for $\tau \to 0$. Starting from (see p. 175 in ref. [24])

$$Q_\nu(x) = \tfrac{1}{2}P_\nu(x)\left(\log\left(\frac{x+1}{x-1}\right) - 2\gamma - 2\frac{\Gamma'}{\Gamma}(\nu+1)\right) - \frac{\sin\pi\nu}{\pi}\sum_{k=1}^{\infty}\frac{\Gamma(k-\nu)\Gamma(k+\nu+1)}{(k!)^2} \times\left[\gamma+\frac{\Gamma'}{\Gamma}(k+1)\right]\left(\frac{1-x}{2}\right)^k, \quad |1-x|<2 \tag{17}$$

one obtains with (see p. 153 in ref. [24])

$$P_{-\frac{1}{2}-ip}(x) = {}_2F_1(\tfrac{1}{2}+ip, \tfrac{1}{2}-ip; 1; \tfrac{1}{2}(1-x)) = 1 + \frac{\cosh\pi p}{\pi}\sum_{k=1}^{\infty}\frac{|\Gamma(\frac{1}{2}+ip+k)|^2}{(k!)^2} \times\left(\frac{1-x|}{2}\right)^k, \quad |1-x|<2 \tag{18}$$

the expression ($x := \cosh\tau$, $1 \le \cosh\tau < 3$)

$$Q_{-\frac{1}{2}-ip}(\cosh\tau) = -\left[\log\left(\tanh\frac{\tau}{2}\right) + \gamma + \frac{\Gamma'}{\Gamma}(\tfrac{1}{2}-ip)\right] + \frac{\cosh\pi p}{\pi}\sum_{k=1}^{\infty}\frac{|\Gamma(\frac{1}{2}+ip+k)|^2}{(k!)^2} \times\left(\frac{1-\cosh\tau}{2}\right)^k\left[\frac{\Gamma'}{\Gamma}(k+1) - \frac{\Gamma'}{\Gamma}(\tfrac{1}{2}-ip) - \tfrac{1}{2}\log\left(\tanh\frac{\tau}{2}\right)\right], \tag{19}$$

where γ is Euler's constant. In (19) the logarithmic singularity is explicitly separated in the first term. In Euclidean billiards the singularity is proportional to $\ln r$ which corresponds exactly to the singularity in the hyperbolic plane because of $r = \tanh(\tau/2)$. By means of the two equations (15) and (19) the Green's function and its normal derivative can be effectively computed. The coefficients in the series are independent of τ and thus can be computed for a fixed energy E or momentum p before the boundary integrals are evaluated, in which only the τ-dependence of $G_0(z, z', E)$ enters. For very highly excited states it suffices to use the asymptotic behaviour

$$Q_{-1/2-ip}(\cosh\tau) \sim \sqrt{\frac{\pi}{2p\sinh\tau}}\,e^{ip\tau+\pi/4} \quad \text{for } p\to\infty \text{ and } \tau \gg \pi/p. \tag{20}$$

However, in general (20) is by far less accurate than the other two expressions.

For the numerical solution of eq. (11), the boundary $\partial\mathcal{F}$ is discretized into intervals of length $\Delta\tau \simeq \pi/2p$, i.e. one de Broglie wavelength is divided into four intervals. On each interval the wavefunction $\Psi(z)$ as well as its normal derivative $\partial\Psi(z)/\partial n$ are approximated by a polynomial $u(\xi)$ of order 3

$$u(\xi) = \sum_{k=1}^{4} u_k N_k(\xi),$$
$$N_1(\xi) = (1-\xi)^2(1+2\xi) = N_3(1-\xi),$$
$$N_2(\xi) = \xi(1-\xi)^2 = -N_4(1-\xi), \tag{21}$$

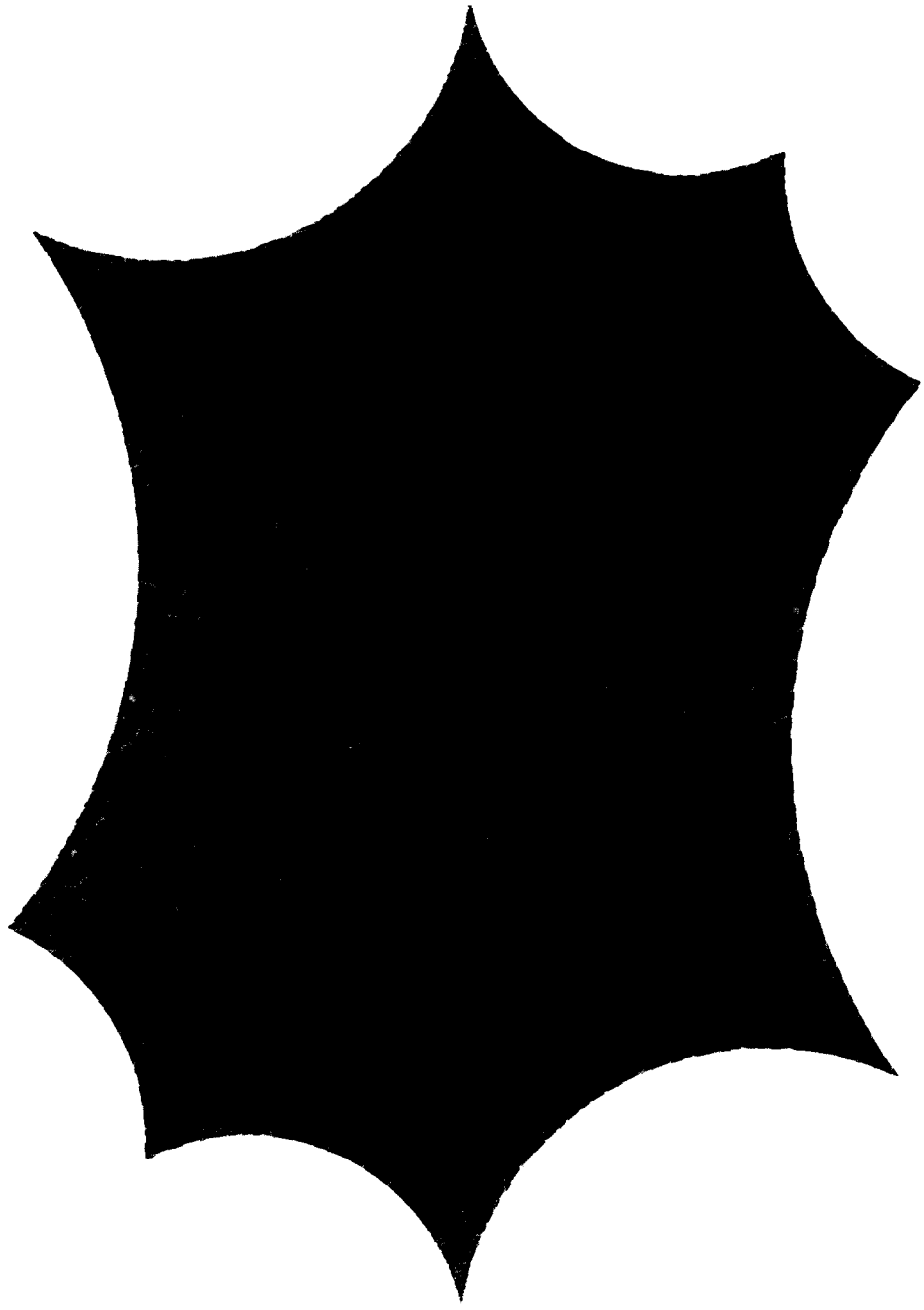

Fig. 1. The intensity $|\Psi_n(z)|^2$ for the eigenstate at energy $E = 2000.695$.

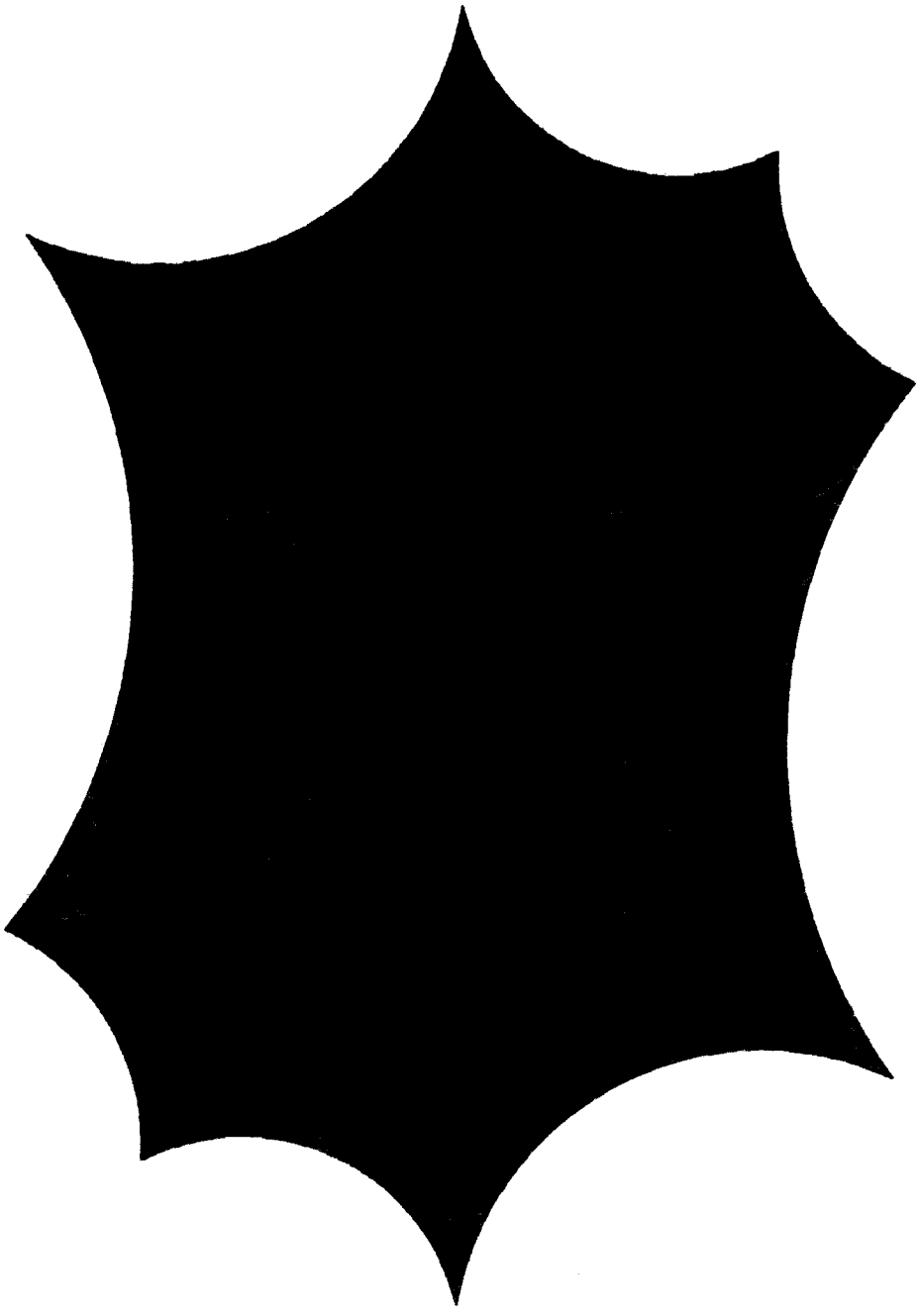

Fig. 2. The intensity $|\Psi_n(z)|^2$ for the eigenstate at energy $E = 2003.117$.

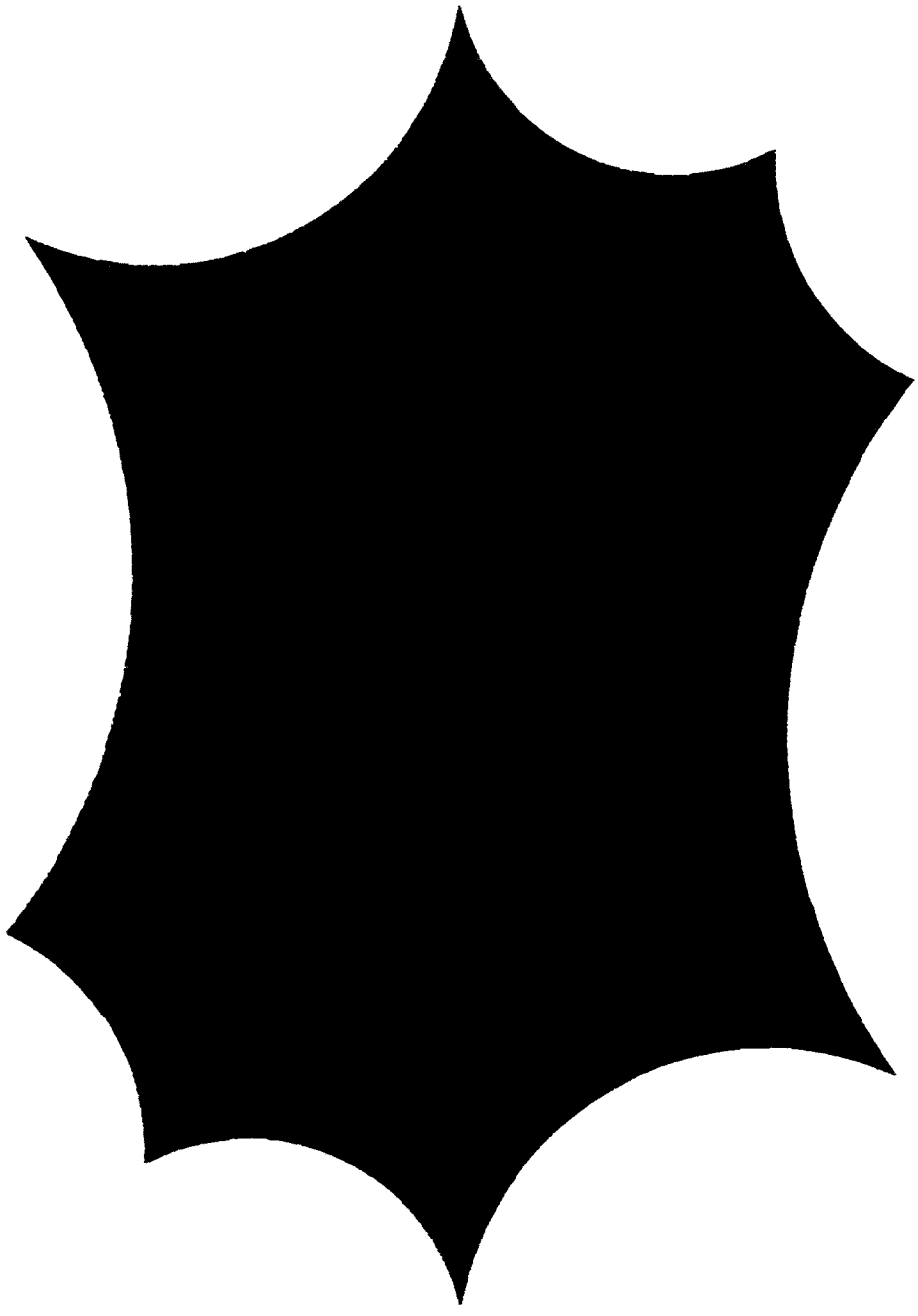

Fig. 3. The intensity $|\Psi_n(z)|^2$ for the eigenstate at energy $E = 10\,001.092$.

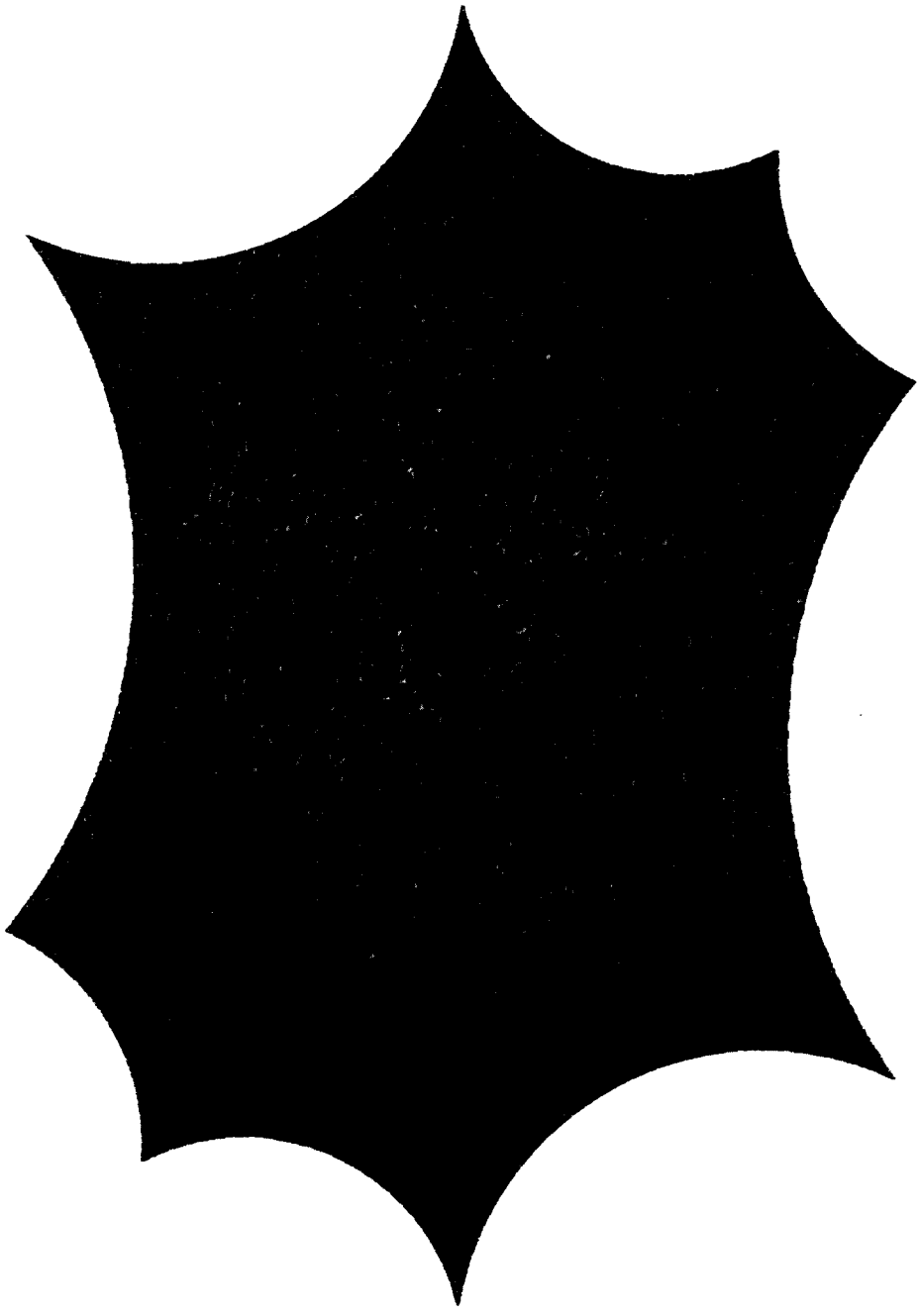

Fig. 4. The intensity $|\Psi_n(z)|^2$ for the eigenstate at energy $E = 10\,003.405$.

where $\xi \in [0, 1]$ is the parametrization of a given interval. With these approximations the integral equation (11) turns into a system of linear equations for the expansion coefficients u_k. However, not all u_k's are independent because of the periodic boundary condition (6). After expressing the system of linear equations only in terms of the independent coefficients u_k, the system will become singular if the energy E in (11) is equal to an eigenvalue E_n of the Schrödinger equation (4). In this way, the eigenvalues can be found and, in addition, using the singular-value decomposition method, also the eigenvectors, i.e. the value of the wavefunction and its normal derivative along the boundary $\partial\mathcal{F}$. Knowing the wavefunction and its normal derivative on the boundary, $\Psi(z)$ can be computed via eq. (11) for all $z \in \mathcal{F}$. Because of the employment of polynomials of order 3, a high convergence is assured enabling us to compute extremely high excited states up to $n = 20\,000$. In the energy range from $E = \frac{1}{4}$ up to roughly $E \simeq 200$ where the boundary-element method as well as the finite-element method can be applied, we have compared the quantal energies and the wavefunctions obtained from the two methods and found that both yield the same results within the numerical accuracy.

In this paper all computations are carried out for an asymmetric hyperbolic octagon which is uniquely defined by the following 4 corner-points $z_k = r_k\, e^{i\varphi_k}$: $r_1 = 0.9405185836$, $\varphi_1 = 0$, $r_2 = 0.8701653$, $\varphi_2 = 0.8023654$, $r_3 = 0.7609273$, $\varphi_3 = 2.1175027$, $r_4 = 0.8575482$, $\varphi_4 = 2.5846103$, where the other 4 corner-points are obtained from these by the parity transformation $z \to -z$. The construction of the complete hyperbolic octagon can then be carried out according to the method outlined in ref. [6]. The eigenstates can be classified by their parity which is the only symmetry an asymmetric octagon can possess. We have computed all eigenstates of positive parity in the energy intervals [2000, 2050], [10 000, 10 020] and [20 000, 20 010]. In figs. 1–4 the intensity structures of four eigenstates with positive parity are shown in the Poincaré disc whose boundary $|z| = 1$ is presented by the red circle. The intensity increases from red hues over yellow towards blue. One observes that the reddish hues are prevailing in contrast to blue hues which is due to the fact that $\Psi(z)$ itself is Gaus-

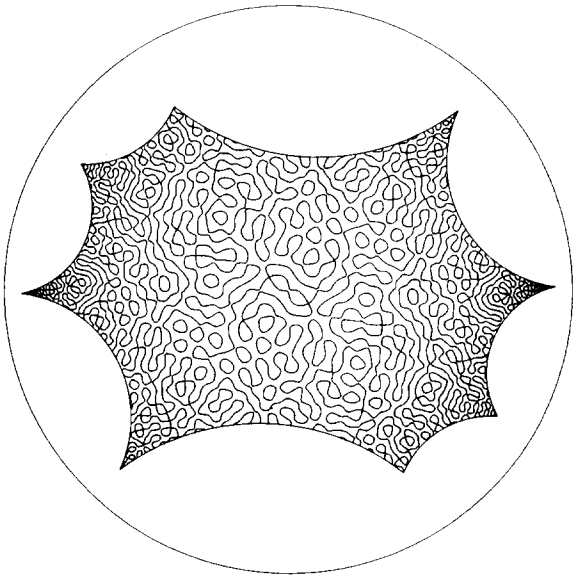

Fig. 5. The nodal lines for the eigenstate at energy $E = 2000.695$.

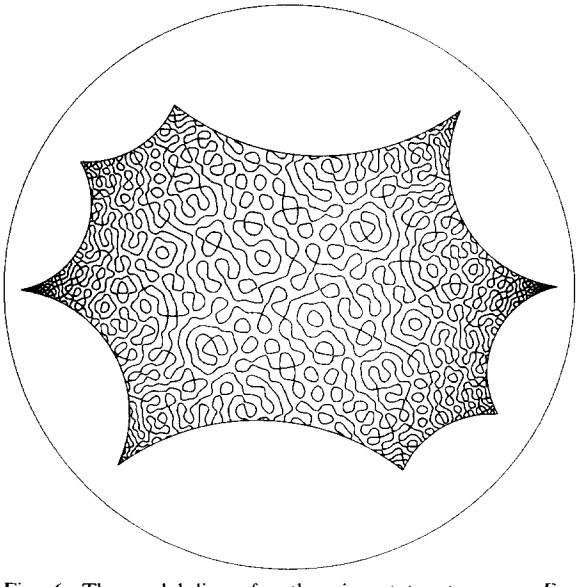

Fig. 6. The nodal lines for the eigenstate at energy $E = 2003.117$.

sian distributed with zero mean (see section 4). Thus high intensities occur relatively seldom. In addition, we present in figs. 5–8 the nodal lines of the same four eigenstates as shown in figs. 1–4. The four examples represent typical members of the set of wavefunctions we have studied.

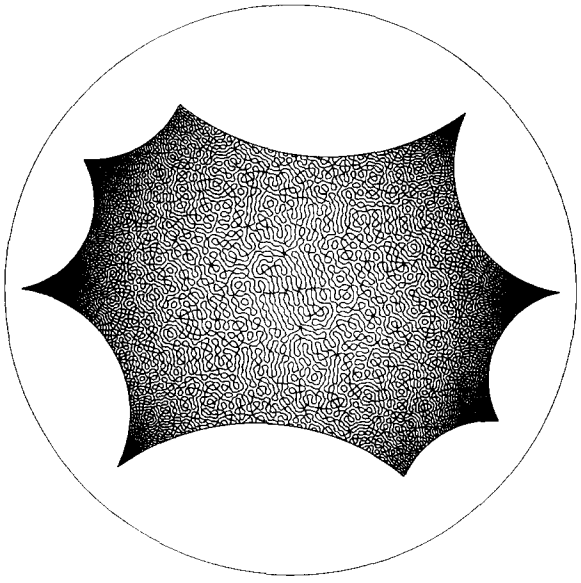

Fig. 7. The nodal lines for the eigenstate at energy $E = 10\,001.092$.

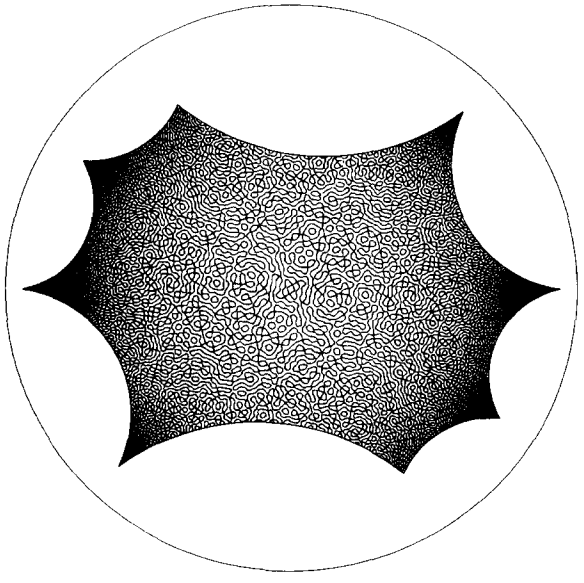

Fig. 8. The nodal lines for the eigenstate at energy $E = 10\,003.405$.

Figs. 1–8 demonstrate clearly the high degree of complexity of chaotic wavefunctions.

3. Statistical properties of eigenstates

As discussed in the last section, the boundary-element method yields primarily the values of the wavefunction and its normal derivative along the boundary. For the following analysis it would be most desirable to have a representation in which the eigenstates are expanded in an orthonormal basis on the fundamental domain $\mathcal{F}$. However, it is practically impossible to construct such a basis because the hyperbolic octagons have no integrable limit from which one could start. To circumvent this problem, we notice that the wavefunctions can be continued to the whole Poincaré disc $\mathcal{D}$ because of the periodic boundary condition (6). Without the condition (6), the motion on the whole disc is integrable and thus allows to express the quantum states in terms of some special functions. In ref. [21] the circular-wave expansion and the plane-wave expansion are discussed and the transformation theory between these two is studied. Here we choose the circular-wave expansion which naturally emerges by considering the Schrödinger equation (4) in hyperbolic polar coordinates (τ, ϕ) with $z = \tanh(\tau/2)\,\mathrm{e}^{\mathrm{i}\phi}$, $0 \le \tau < \infty$, $0 \le \phi \le 2\pi$. This expansion reads

$$\Psi(z) = \sum_{m=-\infty}^{\infty} \hat{a}_m F_m(s, \tau)\,\mathrm{e}^{\mathrm{i}m\phi}$$
$$\text{with } F_m(s,\tau) := (-1)^m$$
$$\times \left|\frac{\Gamma(s)}{\Gamma(s+m)}\right| P^m_{-s}(\cosh\tau)\,, \qquad (22)$$

where $P^m_\nu(x)$ is the associated Legendre function defined in the complex x-plane cut along the interval $[-1, +1]$, and s is determined by the energy E via $s = \frac{1}{2} - \mathrm{i}p$. Notice that the eigenvalues E_n of the Schrödinger equation (4) are given by $E_n = s_n(1 - s_n) = p_n^2 + \frac{1}{4}$, $s_n = \frac{1}{2} - \mathrm{i}p_n$.

The functions $F_m(s,\tau)$ are real for $s=\frac{1}{2}-\mathrm{i}p$, $p\in\boldsymbol{R}$, $0\le\tau<\infty$. In contrast to $P^m_{-s}(\cosh\tau)$, the function $F_m(s,\tau)$ is scaled in such a way that the normalization integral over the Poincaré disc $\mathscr{D}$ is independent of the index m

$$\int_0^\infty F_m(s,\tau)\,F_m(s',\tau)\sinh\tau\,\mathrm{d}\tau = \frac{p\tanh\pi p}{4\pi^2}\,\delta(p-p')\,, \tag{23}$$

for $s=\frac{1}{2}-\mathrm{i}p$, $s'=\frac{1}{2}-\mathrm{i}p'$, $p,p'\in\mathbb{R}$, as can be read off from

$$\int_0^\infty P^m_{-s}(\cosh\tau)\,P^m_{-s'}(\cosh\tau)\sinh\tau\,\mathrm{d}\tau = \frac{p\tanh\pi p}{4\pi^2}\left|\frac{\Gamma(s+m)}{\Gamma(s)}\right|^2\delta(p-p')\,, \tag{24}$$

where $\sinh\tau\,\mathrm{d}\tau$ is due to the invariant volume element of the hyperbolic metric (3). To address the question of localization with respect to some generic basis, it is important that the normalization is independent of the expansion index. In RMT this is achieved by the normalization of each basis vector to unity, which is impossible in our case, because our basis does not refer to the hyperbolic octagon $\mathscr{F}$, but rather is defined on the whole Poincaré disc $\mathscr{D}$, which is infinitely extended and permits only a δ-function normalization. In the case of non-localized eigenstates with respect to the circular-wave expansion, one expects expansion coefficients $\hat{a}_m$ of the same magnitude.

For a given hyperbolic octagon, the circular-wave expansion seems to provide a generic basis since the periodic boundary condition (6) is not reflected by this basis. This is a crucial point because the considered hyperbolic octagon is defined by an arbitrarily chosen periodic boundary condition from a set of infinitely many possibilities, and all these possibilities would be described by the same basis which thus cannot have a special connection to a given hyperbolic octagon.

The eigenfunctions of hyperbolic octagons are always real and possess parity symmetry. In this paper we consider only eigenstates with positive parity, i.e. $\Psi(z)=\Psi(-z)$, in which case the expansion (22) can be simplified to

$$\Psi(z)=\tfrac{1}{2}a_0F_0(s,\tau)+\sum_{n=1}^{\infty}\left[a_{2n-1}\sin(2n\phi)+a_{2n}\cos(2n\phi)\right]F_{2n}(s,\tau)\,. \tag{25}$$

The (new) real expansion coefficients a_n can be computed from a given wavefunction with positive parity and energy $E=s(1-s)=p^2+\frac{1}{4}$ by Fourier analysis ($z=r\,\mathrm{e}^{\mathrm{i}\phi}$, $r=\tanh(\tau/2)$)

$$\frac{2}{\pi}\int_0^\pi \mathrm{d}\phi\,\Psi(r\,\mathrm{e}^{\mathrm{i}\phi})\cos(2n\phi) = F_{2n}(s,\tau)a_{2n}\,, \tag{26}$$

$$\frac{2}{\pi}\int_0^\pi \mathrm{d}\phi\,\Psi(r\,\mathrm{e}^{\mathrm{i}\phi})\sin(2n\phi) = F_{2n}(s,\tau)a_{2n-1}\,. \tag{27}$$

In principle, these equations allow the determination of the coefficients a_n independently of an arbitrary value of r. However, the maximal index $n_{\max}$, for which the a_n's can be computed with sufficient numerical stability, is determined by a property of the functions $F_n(s,\tau)$ which carries over from the Legendre functions. The function $F_n(s,\tau)$ vanishes rapidly in the classically forbidden region $\sinh\tau<n/p$ [21]. For values of n which are bigger than $n_{\max}$, the small values of $F_n(s,\tau)$ cause numerical instabilities in the computation of the a_n's. We therefore restrict ourselves to the a_n's with $n\le n_{\max}$ which belong to circular waves in the classically allowed region. With $r=\tanh(\tau/2)$ we obtain

$$n_{\max}:=p\sinh\tau=\frac{2pr}{1-r^2}\,. \tag{28}$$

In our computations we use $r \in [0.94, 0.95]$, and with $r = 0.9475$ one obtains from (28) the limits $n_{\max} \simeq 829$, $n_{\max} \simeq 1853$ and $n_{\max} \simeq 2621$ for $E \simeq 2000$, 10 000 and 20 000, respectively. For safety reasons, the following statistics concerning the a_n's are based on 800, 1750 and 2400 coefficients for $E \simeq 2000$, 10 000 and 20 000, respectively.

To get an idea about what could be expected for the statistical properties of the coefficients a_n, consider the predictions of random-matrix theory. Because the hyperbolic octagons possess time-reversal symmetry, one expects that the statistical properties are described by matrices of the Gaussian orthogonal ensemble (GOE). In ref. [6] we have shown that the short-range correlations in the quantal energy spectra are indeed in good agreement with the GOE predictions, but that the long-range correlations have to be modified by the periodic-orbit theory, see also ref. [25]. It is thus a priori not clear whether the GOE predictions are valid for a single eigenstate of a hyperbolic octagon.

The main prediction of RMT for the eigenfunctions is that their expansion coefficients with respect to a generic basis are Gaussian distributed [8]. For the Gaussian unitary ensemble the complex coefficients are considered to be described independently for the real and imaginary parts by a Gaussian distribution. It is convenient to consider the distribution of $|a_n|^2$ instead of a_n, whose distribution is then given by the so-called χ^2_ν distribution

$$p_\nu(x) = \frac{(\nu/2)^{\nu/2}}{\Gamma(\nu/2)}\, x^{\nu/2-1}\, \mathrm{e}^{-\nu x/2}, \tag{29}$$

where

$$x = \frac{1}{\nu\sigma^2} \sum_{i=1}^{\nu} (X_i - \bar{a})^2$$

is the sum of ν independent Gaussian random variables X_i with mean $\bar{a}$ and variance σ^2. In refs. [26,9] agreement with the RMT prediction has been shown in the case of the kicked top for the three universality classes of the orthogonal (GOE, $\nu = 1$), unitary (GUE, $\nu = 2$) and symplectic (GSE, $\nu = 4$) ensemble. The transition towards the integrable case is suspected to correspond to the limit $\nu \to 0$. But this is still a matter of discussion because this behaviour is not reflected in the case of the kicked top [9]. On the other hand, in the case of the coupled-rotators model the transition from chaotic to integrable behaviour can be described by the transition from $\nu = 1$ towards $\nu = 0$ [27].

In the following we want to check whether the coefficients a_n are distributed according to the RMT distribution (29). Note, however, that RMT is not applicable to our case because every wavefunction is expanded in another basis which depends on the momentum p. In the framework of RMT one supposes instead that all eigenstates are expanded in a common basis; but, as mentioned above, this is practically impossible in our case. Thus our hypothesis that the a_n's are distributed according to (29), is based only on an analogy argument.

Let us now turn to the statistical properties of the coefficients a_n. The mean $\bar{a}$ of the coefficients is within the statistical significance in agreement with a zero mean. Before the statistical analysis is carried out, the coefficients are rescaled such that their variance obeys $\sigma^2 = 1$. In fig. 9 we show the obtained cumulative distributions which are, in contrast to histograms, free of the arbitrariness of choosing some bins. Another advantage of the cumulative distributions is that statistical fluctuations are smoothed out, which would be more pronounced in the case of histograms. The cumulative RMT predictions

$$I(x) = \int_0^x \mathrm{d}x'\; p_\nu(x') = \gamma(\tfrac{1}{2}\nu, \tfrac{1}{2}\nu x)/\Gamma(\tfrac{1}{2}\nu) \tag{30}$$

following from (29) are also shown in fig. 9 for the three universality classes. ($\gamma(x, y)$ is the incomplete gamma function). To these distributions we have applied the Kolmogorov–Smirnov

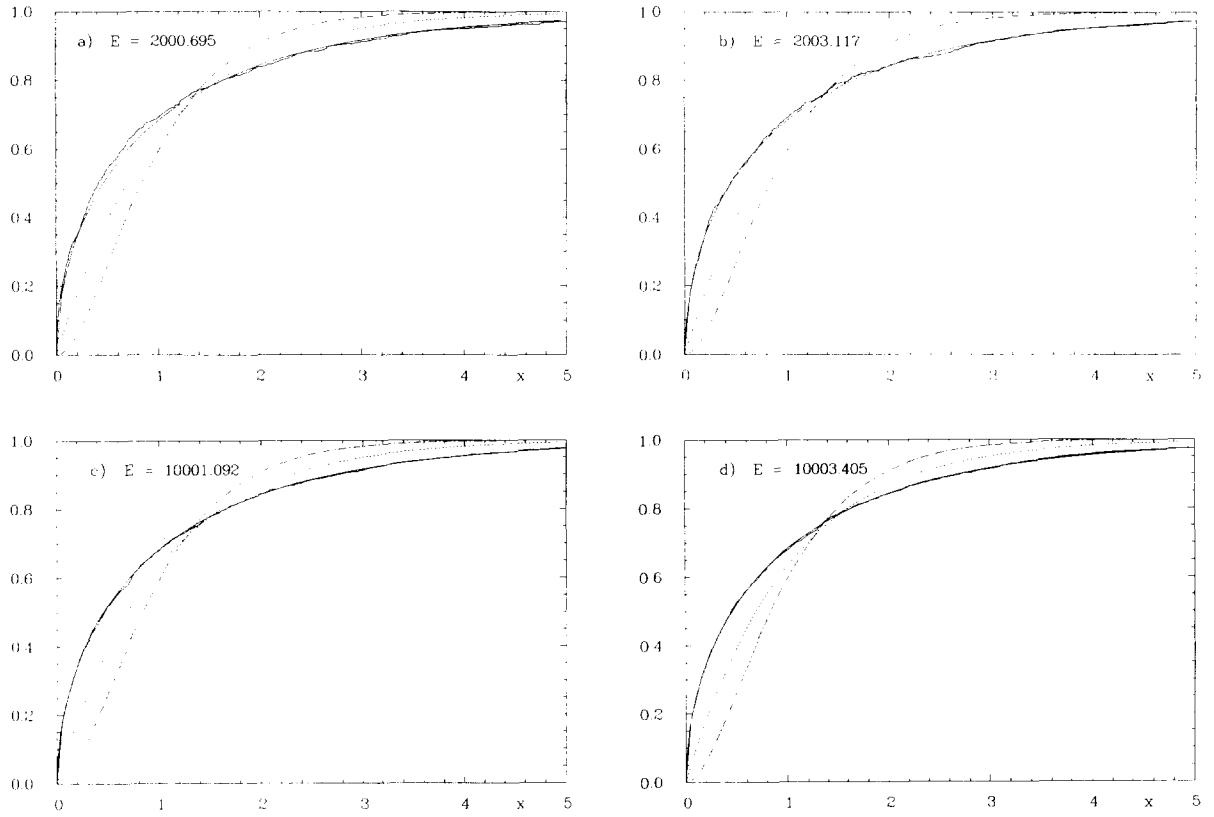

Fig. 9. The cumulative distributions of the coefficients $|a_n|^2$ are shown for four eigenstates in comparison with the RMT expectations for GOE (full curve), GUE (dotted curve) and GSE (dashed-dotted curve). The statistics are based on 800 coefficients in (a) and (b) and on 1750 coefficients in (c) and (d).

test (see e.g. ref. [28]) which yields the approximate significance level $\mathcal{P}$ of the maximal distance D between the cumulative distribution and the theoretical prediction, i.e. $\mathcal{P}$ is the probability to obtain a maximal distance D greater than the observed one. These significance levels $\mathcal{P}$ with respect to the GOE prediction are listed in table 1 for the four eigenstates shown in fig. 9 and, in addition, for some other eigenstates which have been studied. In all cases one observes high significance levels $\mathcal{P} \gg 1\%$ which demonstrates a remarkably good agreement with the prediction (30) for $\nu = 1$. Even the worst significance level with $\mathcal{P} = 4.9\%$ in the case of the eigenstate at $E = 10\,015.617$ lies well in the acceptable range.

Next we want to discuss the question whether the circular waves are uniformly distributed. For that purpose we rewrite eq. (25) as follows:

$$\Psi(z) = \frac{a_0}{2} F_0(s, \tau) + \sum_{n=1}^{\infty} A_n \sin(2n\phi + \vartheta_n) F_{2n}(s, \tau) , \qquad (31)$$

with

$$A_n := \sqrt{a_{2n-1}^2 + a_{2n}^2}$$

and $\tan \vartheta_n := a_{2n}/a_{2n-1}$.

From the assumption that the a_n's of the expansion (25) behave as independent Gaussian variables, one can calculate the prediction for the

Table 1
The significance levels $\mathcal{P}$ of the cumulative distributions $I(x)$, $I(\vartheta)$ and $I(A)$ with respect to the theoretical predictions discussed in the text are listed according to the Kolmogorov–Smirnov test.

E_n	$\mathcal{P}$ for $I(x)$	$\mathcal{P}$ for $I(\vartheta)$ with $\theta \in [-\pi, \pi]$	$\mathcal{P}$ for $I(\vartheta)$ with $\vartheta \in [-\frac{1}{2}\pi, \frac{1}{2}\pi]$	$\mathcal{P}$ for $I(A)$
2,000.695	28.5%	50.0%	30.6%	93.7%
2,003.117	93.8%	94.9%	94.3%	85.3%
2,005.110	69.4%	79.2%	33.6%	40.7%
2,007.536	82.9%	96.2%	92.7%	96.7%
2,009.041	99.9%	77.4%	17.9%	86.6%
10,001.092	86.0%	7.8%	62.1%	49.8%
10,003.405	99.0%	18.1%	63.2%	53.4%
10,005.463	52.3%	15.1%	30.7%	97.4%
10,006.061	58.1%	34.6%	29.2%	28.3%
10,008.095	41.4%	5.3%	2.3%	67.2%
10,011.254	51.8%	63.3%	82.3%	98.7%
10,013.180	44.5%	57.8%	3.9%	22.9%
10,013.697	34.5%	16.2%	34.8%	60.8%
10,015.617	4.9%	70.2%	51.2%	60.7%
10,016.972	81.6%	74.0%	97.6%	80.3%
10,019.897	93.2%	94.3%	56.4%	42.0%
20,001.170	62.0%	28.2%	33.1%	28.3%
20,004.057	94.5%	65.9%	77.2%	91.1%
20,004.915	69.4%	43.4%	82.3%	69.1%
20,007.327	77.2%	47.8%	84.1%	83.2%
20,008.391	35.4%	99.2%	85.8%	29.2%
20,009.745	66.1%	91.1%	9.0%	56.7%

amplitudes A_n and the phases ϑ_n of the expansion (31). The numerical test of these predictions allows to check the independence of a_{2n-1} from a_{2n} which is an important ingredient in the following computation of the probability distributions $P(\vartheta)$ and $P(A)$.

Because a_{2n-1} and a_{2n} are assumed to be independent, the probability distribution of their quotient $q = a_{2n}/a_{2n-1}$ is determined by

$$P_{12}(q) = \int_{-\infty}^{\infty} \mathrm{d}x\, |x|\, P_1(qx)\, P_2(x)\,, \tag{32}$$

being valid for the quotient of two independent variables drawn from the distributions P_1 and P_2, respectively. For a Gaussian distribution with $\sigma^2 = 1$ one arrives with (32) at the Cauchy distribution

$$P(q) = \frac{1}{\pi}\,\frac{1}{1+q^2}\,. \tag{33}$$

If one considers the distribution of ϑ_n in the restricted interval $[-\frac{1}{2}\pi, \frac{1}{2}\pi]$, one can convert the probability $P(q)$ via $q := \tan\vartheta$ whereby one ends up with $P(\vartheta) = \frac{1}{4}$ predicting the isotropy of the circular waves in this restricted interval. This result agrees with the intuitive picture of a strongly chaotic system having eigenstates stochastically composed of generic basis states. Numerically we find isotropy in the full interval $[-\pi, \pi]$ as demonstrated in fig. 10 for the same eigenstates as in fig. 9. The cumulative distribution $I(\vartheta) = \int_{-\pi}^{\vartheta} \mathrm{d}\vartheta'\, P(\vartheta')$ is shown in comparison with the straight line corresponding to an isotropic distribution. The significance levels $\mathcal{P}$ of the Kolmogorov–Smirnov test are again given in table 1. The largest deviation from the isotropic distribution occurs in the case of the eigenstate at $E = 10\,001.092$ (fig. 10c) and it has a somewhat low significance level $\mathcal{P}$ in turn. A look at table 1 shows, however, that the other eigenstates studied have, with the exception of

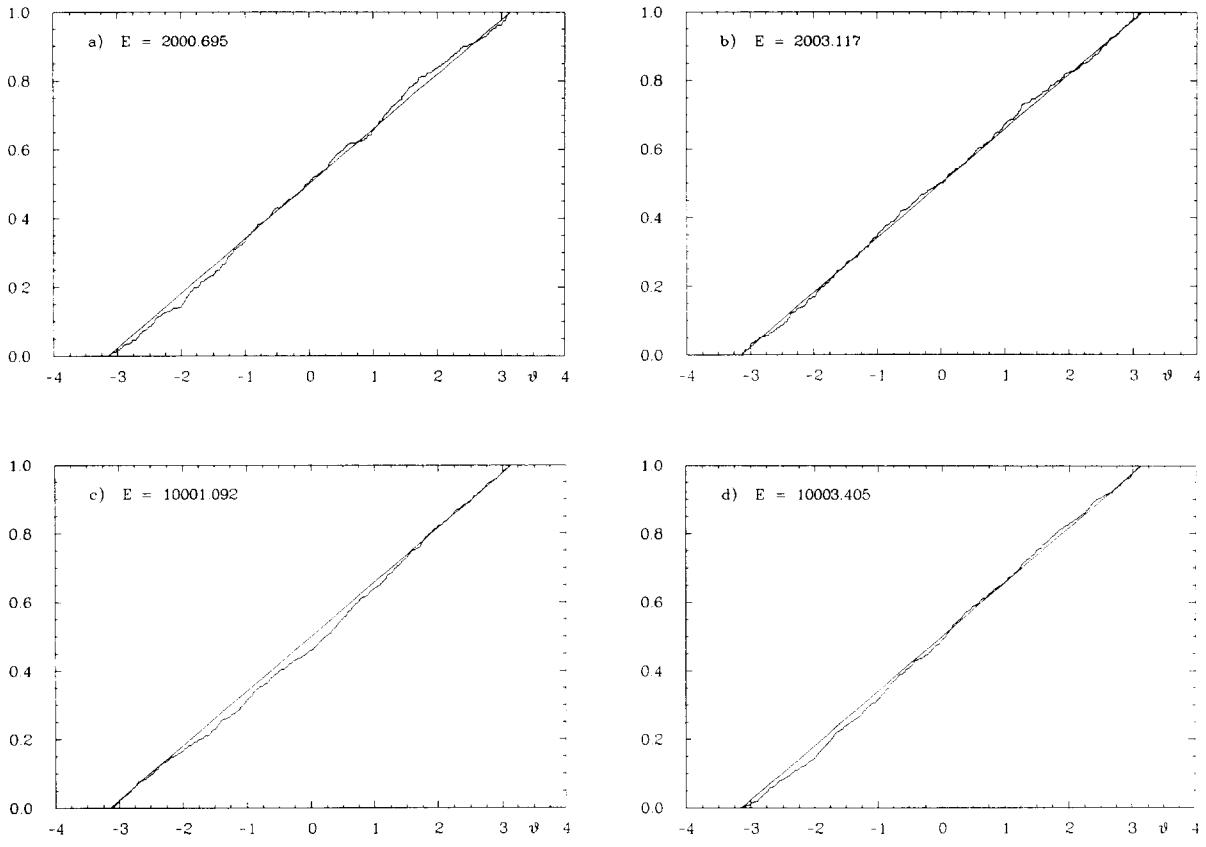

Fig. 10. The cumulative distribution of the phases $\vartheta_n \in [-\pi, \pi]$ is shown in comparison with the isotropic expectation (straight line).

the one at $E = 10\,0008.095$, higher significance levels $\mathcal{P}$. In addition we list in table 1 also the significance levels $\mathcal{P}$ obtained from the cumulative distribution over the interval $[-\frac{1}{2}\pi, \frac{1}{2}\pi]$ displaying also acceptable significance levels.

The distribution of the coefficients A_n in the expansion (31), which will play a crucial role in the description of the correlation properties of the eigenstates (see section 5), can be obtained in a similar way. Assuming $x := a_{2n-1}^2$ and $y := a_{2n}^2$ to be independent random variables with variance $\sigma^2 = 1$, the distribution $P(s)$ of the sum $s = x + y$ is obtained by the convolution of the distributions P_1 and P_2 from which x and y are drawn

$$P(s) = \int_{-\infty}^{\infty} \mathrm{d}x\, P_1(x)\, P_2(s - x) = \tfrac{1}{2}\, \mathrm{e}^{-s/2}\,, \quad s \geq 0\,,$$

where we have assumed that P_1 and P_2 are equal to the distribution (29) with $\nu = 1$. Converting this probability distribution to the variable $A = \sqrt{s}$ leads to the result

$$P(A) = A \exp(-A^2/2)$$
$$\text{and thus } I(A) = 1 - \exp(-A^2/2)\,. \tag{34}$$

In fig. 11 we show the cumulative distribution $I(A) = \int_0^A \mathrm{d}A'\, P(A')$ in comparison with the pre-

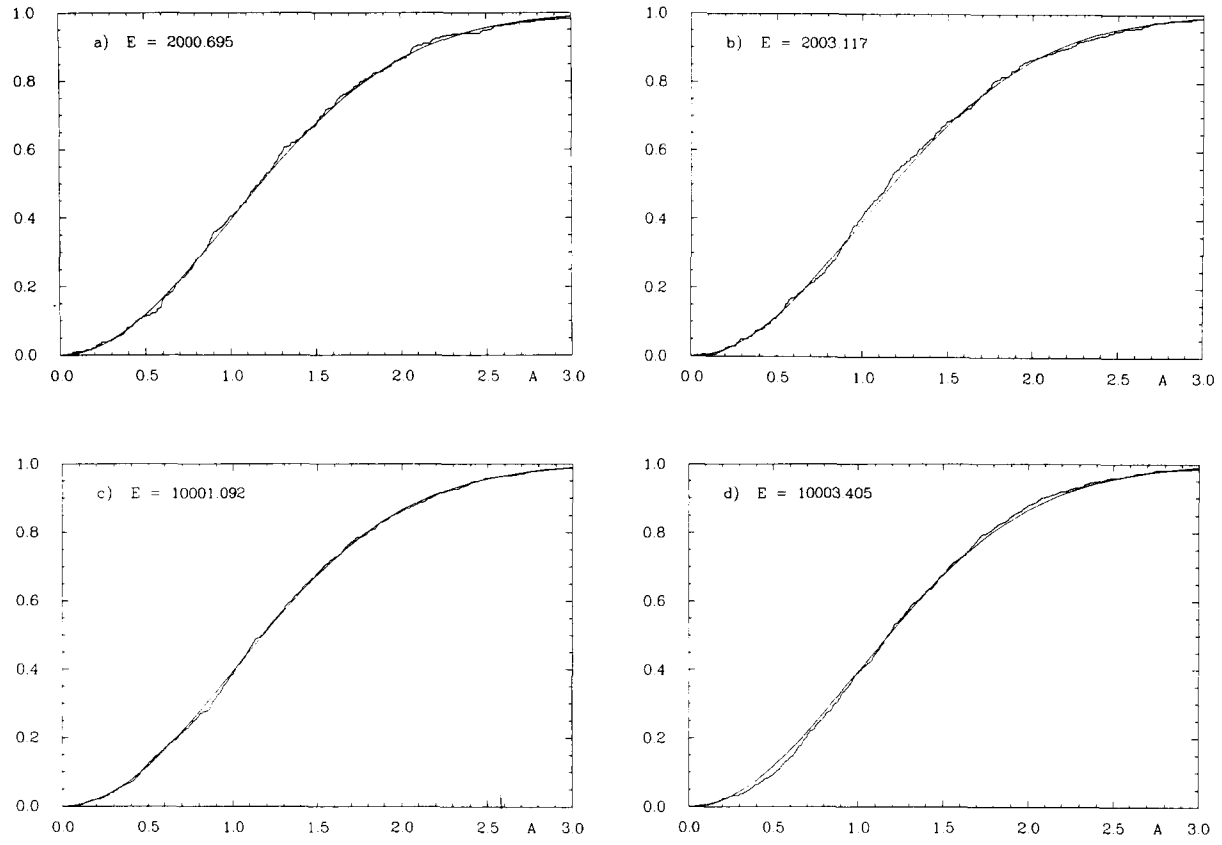

Fig. 11. The cumulative distribution of the amplitudes A_n is shown in comparison with the theoretical expectation $I(A) = 1 - \exp(-A^2/2)$ (full line).

diction (34). For all four eigenstates one observes good agreement with (34) together with high significance levels $\mathcal{P}$, which are again listed in table 1 together with the significance levels for the other eigenstates studied. The expansion (31) exemplifies clearly that the statistic of the expansion coefficients has not always to obey a Gaussian behaviour but rather depends on the specific basis which has been chosen.

It is clear that the observed Gaussian distribution of the coefficients a_n rules out a localization in the circular-wave basis. As already pointed out above, the considered circular-wave expansion is correctly normalized to address this question. In fig. 12a the expansion coefficients a_n are shown in the range $n \in [0, 2000]$ for the eigenstate at $E = 10\,003.405$, and the absence of localization is again well demonstrated. Up to now we have only studied the distribution itself and possible correlations between a_{2n-1} and a_{2n}. However, to consider the coefficients as pseudo-random numbers, it is important that there are no correlations over longer ranges.

That such correlations could occur in principle, is shown by the following consideration. Assume that one has calculated all the coefficients a_n by evaluating eqs. (26) and (27) on a circle with radius r_1 which encloses the fundamental domain. As described above in connection with eq. (28), for very large n the coefficients a_n cannot be computed since the functions $F_n(s, \tau)$ are numerically too close to zero.

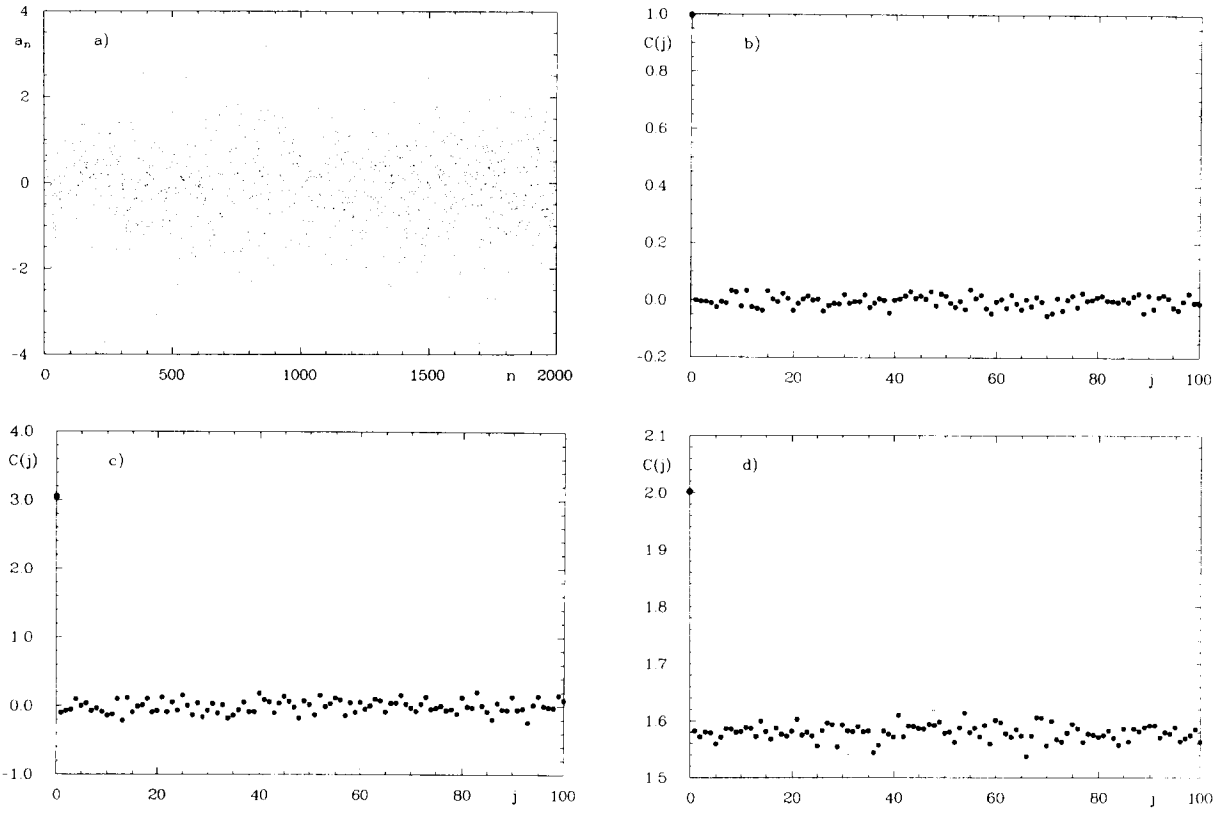

Fig. 12. In (a) the first 2000 coefficients are shown for the eigenstate at $E = 10{,}003.405$. In (b), (c) and (d) we present the correlations for the coefficients a_n, the phases ϑ_n and the amplitudes A_n, respectively.

Now consider a second circle with radius $r_2 > r_1$. The wavefunction on the circle with radius r_2 can be expressed by the coefficients obtained from the circle with radius r_1, since all points on the circle with radius r_2 can be transformed by the periodic boundary condition (6) to points lying inside the circle with radius r_1, where the coefficients obtained from the circle with radius r_1 suffice to describe the wavefunction. Thus one obtains infinitely many equations which express the $n_{\max}(r_2)$ coefficients by the $n_{\max}(r_1)$ coefficients, and because of $n_{\max}(r_2) > n_{\max}(r_1)$ one can in principle compute additional coefficients a_n from the coefficients known from the circle at radius r_1. Thus one cannot exclude a priori that some correlations among the a_n's arise as a consequence of these equations. It may be that these "recursion" relations possess properties analogous to the well-known recursion relation $a_{n+1} = xa_n (\mathrm{mod}\ y)$ with x and y fixed, which are used by computers in generating pseudo-random numbers. Such recursion relations are well studied in the case of some maps in connection with chaotic systems, e.g. the Bernoulli shift in one dimension or Baker's map in two dimensions. They depend extremely sensitively on the "initial" condition a_0 and no correlations arise.

To be more rigorous, we study the following measure for the correlations among the coefficients

$$C(j) = \frac{1}{N} \sum_{i=1}^{N} a_i a_{i+j} \,. \tag{35}$$

For random numbers with zero mean one expects $C(0) = \overline{a_n^2}$ and $C(j) = 0$ for $j > 0$. Again for

the eigenstate at $E = 10\,003.405$, the correlation of the first 2000 coefficients a_n of the circular-wave expansion (25) is shown in fig. 12b. One observes $C(0) = 1$ and $C(j) \simeq 0$ for all other values of j thus demonstrating the character of the a_n's as pseudo-random numbers. In figs. 12c and 12d the correlations of the phases ϑ_n and the amplitudes A_n, respectively, of the expansion (31) are displayed showing again no correlations.

Thus the coefficients a_n as well as the phases ϑ_n and the amplitudes A_n fit well into the RMT scheme. Because they are uncorrelated, they behave as pseudo-random numbers. We prefer the term "pseudo-random" to "random" because they are not exactly random in the mathematical sense, since they are constrained by the Schrödinger equation in an analogous way as the formulae are which are used by computers in generating pseudo-random numbers.

4. The amplitude distribution $P(\Psi)$

Up to now we have only discussed the statistical properties of the expansion coefficients of the eigenstates with respect to the circular-wave expansion. Let us now turn to the statistical properties of the eigenstates themselves. In this section we want to discuss one of the simplest statistics, the amplitude distribution $P(\Psi)$, which describes the distribution of the wavefunction Ψ itself.

To contrast the properties of chaotic systems with the ones of integrable systems, let us first recall some facts about integrable systems. The classical motion of integrable systems with N degrees of freedom takes place on N-tori embedded in the $2N$-dimensional phase space due to the N classical constants of motion. The semiclassical approximation for the wavefunctions can be obtained from the WKB approximation by applying this method separately on each of the N irreducible circuits on the N-tori. Then the complete semiclassical approximation of the wavefunction is composed of primitive WKB approximations. Semiclassically, the wavefunction thus consists of N oscillatory contributions from the N-tori. (This simple view must, however, be modified by the singularities of the Van Vleck determinant occurring on the caustics of the system). This contrasts to the case of chaotic systems, where due to the lack of enough constants of motion no such N-tori exist and one thus expects that infinitely many uncorrelated oscillatory contributions determine the wavefunction. This argument led Berry [14] to suggest that the wavefunctions of chaotic systems behave statistically as Gaussian random functions. This random character is absent in the case of integrable systems where the finite number of oscillatory contributions cause an anisotropy in the wavefunction and thus correlations incompatible with the picture of a random function. In addition, a further non-Gaussian contribution arises by the caustics in the integrable case.

The simplest property of a Gaussian random function is that its values Ψ should be distributed as

$$P(\Psi) = \frac{1}{\sqrt{2\pi}\sigma} \, \mathrm{e}^{-(\Psi^2/2\sigma^2)} , \tag{36}$$

where σ^2 is the variance of the distribution being determined by the normalization of the wavefunctions. This distribution was numerically found to be valid for most wavefunctions in the case of the stadium billiard [29,30], which is also strongly chaotic. An exception is played by the so-called bouncing ball modes which are more regular due to the straight line boundaries of the stadium billiard. To contrast this behaviour, the circular billiard being classically integrable was also studied in [30] and the wavefunctions were found to be highly non-Gaussian.

In the last section it was demonstrated that the coefficients a_n of the circular-wave expansion (25) behave as uncorrelated Gaussian random variables. Now we want to show that this fact already implies a Gaussian amplitude distribution $P(\Psi)$ in the semiclassical limit $p \to \infty$. In the

following we restrict ourselves to an annulus with radius τ and width $\Delta\tau \gg 2\pi/p$. The latter condition is necessary to guarantee that the width $\Delta\tau$ is large in comparison with the de Broglie wavelength $\lambda_B = 2\pi/p$. Then it will be shown that on such an annulus $\hat{P}(\Psi)$ is Gaussian distributed in the semiclassical limit $p \to \infty$, and that all annuli contribute with the same variance to the amplitude distribution $P(\Psi)$ of the whole domain.

In the first step one has to compute the amplitude distribution P_{cw} of a single circular wave of the expansion (25), i.e. of a function of the form

$$f_n(\tau, \phi) = a_n \sin(x_n)\, F_n(s, \tau)\,. \tag{37}$$

Here we restrict ourselves to the sine because the cosine also occurring in (25) has the same statistical properties. The distribution $P_G(a)$ of the a_n's is a Gaussian with unit variance as already stated

$$P_G(a) = \frac{1}{\sqrt{2\pi}}\, e^{-a^2/2}\,. \tag{38}$$

The argument of the sine can be considered as a random phase for $n \to \infty$, because the sine function acts as $\mathrm{mod}_{2\pi}$ for $n\phi$ (see eq. (25)). The special cases of $\phi = \pi/m$ with m integer are of measure zero in $[0, 2\pi]$ and do not influence the total distribution. The amplitude distribution $P_{sin}(x)$ of the sine can be shown to be

$$P_{sin}(x) = \frac{1}{\pi}\,\frac{1}{\sqrt{1-x^2}}$$
$$\text{for } |x| < 1 \text{ and } 0 \text{ otherwise}\,. \tag{39}$$

Since we are dealing with the semiclassical limit, we employ for $F_n(s, \tau)$ the semiclassical approximation

$$F_n(s, \tau) = \sqrt{\frac{2}{\pi p \sinh \tau}}\, \sin\left(p\tau + \frac{3\pi}{2}\, n + \frac{\pi}{4}\right)$$
$$\text{for } n \ll p\,. \tag{40}$$

Again one has a sine function, which can be treated like the preceding sine function, because the argument $y_n = p\tau + \frac{3}{2}\pi n + \frac{1}{4}\pi (\mathrm{mod}\, 2\pi)$ can be considered as a random phase. The crucial point is that the amplitudes

$$b_n = \sqrt{\frac{2}{\pi p \sinh \tau}} = b \tag{41}$$

are independent of n for $n \ll p$, which is a consequence of the normalization (23) where the factor $\sinh \tau$ arising from the hyperbolic metric is cancelled by b_n. The amplitude distribution $P_{F_n}(f)$ of the $F_n(s, \tau)$ is thus with $n \ll p$ and $p \to \infty$

$$P_{F_n}(f) = \frac{1}{\pi}\,\frac{1}{\sqrt{b^2 - f^2}}$$
$$\text{for } |f| < b \text{ and } 0 \text{ otherwise}\,. \tag{42}$$

Now one can compute the amplitude distribution P_{cw} for the product (37) from the three distributions (38), (39) and (42). Since all of these are symmetric, one can use

$$P_{12}(z) = 2 \int_0^\infty \frac{dx}{x}\, P_1(x)\, P_2(z/x) \tag{43}$$

for the distribution of the product of two independent variables drawn from the distributions P_1 and P_2. Applying (43) to the distributions (38) and (39), one arrives at

$$P_{Gsin}(z) = \frac{e^{-z^2/4}}{\sqrt{2\pi^3}}\, K_0\left(\frac{z^2}{4}\right), \tag{44}$$

where K_0 is the modified Bessel function of order 0. It is worthwhile to note that the distribution (44) is highly non-Gaussian because of $K_0(x) \sim -\ln(\frac{1}{2}x)$ for $x \to 0$. Inserting (44) and (42) in eq. (43), one finally ends up with

$$P_{\mathrm{cw}}(z) = \frac{1}{\sqrt{2b^2\pi^5}} \int_1^\infty \frac{\mathrm{d}x}{\sqrt{x^2 - x}} \exp\left(\frac{-z^2}{4b^2}\, x\right) \times K_0\left(\frac{z^2}{4b^2}\, x\right) = \frac{1}{\sqrt{2b^2\pi^3}}\, G_{23}^{30}\left(\frac{z^2}{2b^2}\,\middle|\, \begin{matrix} \frac{1}{2} & \frac{1}{2} \\ 0 & 0 \quad 0 \end{matrix}\right) \tag{45}$$

where G_{pq}^{mn} is Meijer's G-function (see e.g. ref. [31]). Because the argument is z^2, the distribution has zero mean $\bar{z} = 0$ as it should be, since this is also valid for the original distributions (38), (39) and (42). Despite the complicated Meijer's G-function, the variance

$$\hat{\sigma}^2 = \int_{-\infty}^{\infty} \mathrm{d}z (z - \bar{z})^2\, P(z) \tag{46}$$

can be computed leading to the simple result

$$\hat{\sigma}^2 = \frac{b^2}{4} = \frac{1}{2\pi p \sinh \tau}\,. \tag{47}$$

Thus we get the result that for $p \to \infty$ infinitely many ($n \ll p$) distributions with finite variance $\hat{\sigma}^2$ contribute to the desired amplitude distribution $\hat{P}(\Psi)$ on an annulus. In the framework of the central limit theorem one can prove with the aid of the so-called continuity theorem that the sum of n random variables drawn from a common cumulative distribution $I(x) = \int_{-\infty}^{x} \mathrm{d}x'\, P(x')$ with finite variance σ^2 is in the limit $n \to \infty$ normal (Gaussian) distributed with variance $n\sigma^2$ (see e.g. p. 293 in ref. [28]). (One can also check the validity of the Lindeberg condition for the distribution (45), which is a necessary and sufficient condition for the applicability of the central limit theorem (see p. 294 ff in ref. [28]).) Thus $\hat{P}(\Psi)$ is Gaussian distributed for $p \to \infty$ on an annulus. The variance σ^2 is thus given by the sum of the variances of the contributing N circular waves

$$\sigma^2 = \sum_{n=1}^{N} \hat{\sigma}^2 = \frac{N}{2\pi p \sinh \tau}\,. \tag{48}$$

Since the functions $F_n(s, \tau)$ vanish rapidly in the classically forbidden region $\sinh \tau < n/p$, the number N can be approximated by $N \simeq p \sinh \tau$ and thus $\sigma^2 \simeq 1/2\pi$. This variance is independent of τ and each annulus contributes in the same way to the whole amplitude distribution $P(\Psi)$, which is thus Gaussian distributed with variance $\sigma^2 \simeq 1/2\pi$.

It must be noted that the above variance applies in the case where the expansion coefficients a_n are scaled in such a way that they possess unit variance as was always assumed up to now. However, if one considers wavefunctions normalized on a hyperbolic octagon according to (7), one obtains $\sigma^2 = 1/4\pi$ by assuming a Gaussian $P(\Psi)$. In fig. 13 the cumulative amplitude distribution is shown for the normalized wavefunctions belonging to the same states as in the previous figures. The agreement with the theoretical prediction is so excellent that no deviation is visible within the graphical resolution. As is expected from this agreement, the Kolmogorov–Smirnov test also yields high probabilities $\mathcal{P}$ for a Gaussian distribution with $\sigma^2 = 1/4\pi$, as listed in table 2.

Table 2 also contains the skewness

$$\text{Skewness} = \frac{(4\pi)^{3/2}}{N} \sum_{j=1}^{N} \Psi_j^3$$

and the kurtosis

$$\text{Kurtosis} = \left(\frac{16\pi^2}{N} \sum_{j=1}^{N} \Psi_j^4\right) - 3$$

($\sigma^2 = 1/4\pi$ is assumed) of these distributions, measuring the third and the fourth moment of the distributions. For a Gaussian distribution both should be zero in the limit $N \to \infty$. For an underlying normal distribution, statistical fluctuations cause for large but finite N non-vanishing values with a standard deviation of approximately $\sqrt{6/N}$ for the skewness and $\sqrt{24/N}$ for the kurtosis. In table 2 the quotients of the skewness and kurtosis to their respective stan-

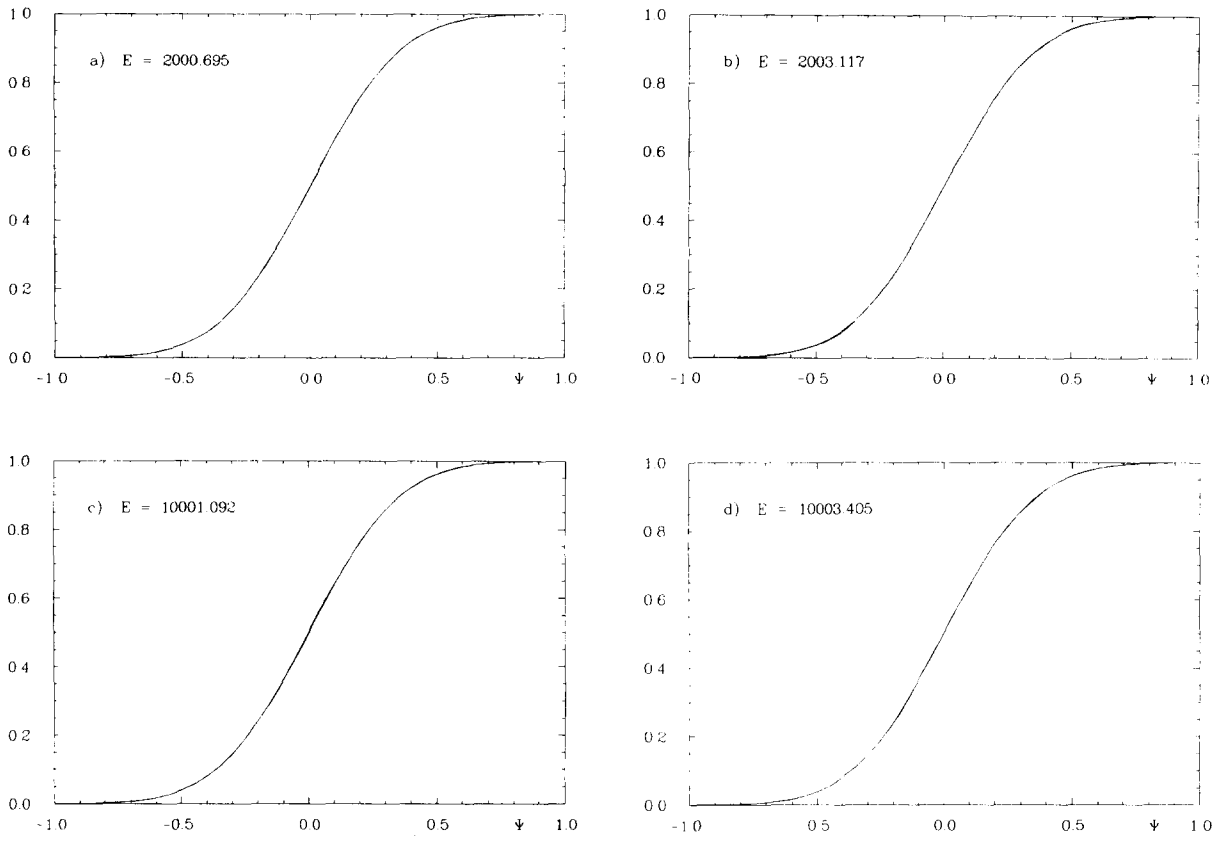

Fig. 13. The cumulative amplitude distribution $I(\Psi)$ is shown in comparison with the theoretical expectation $I(\Psi) = \frac{1}{2} + \frac{1}{2}\mathrm{erf}(\sqrt{2\pi}\Psi)$ for the same eigenstates as in the preceding figures. The statistics consist of 20 000 values for each eigenstate.

dard deviations are also listed, where one observes in no case deviations of more than four standard deviations. Thus even these sensitive measures clearly show the Gaussian behaviour of the amplitude distribution $P(\Psi)$.

We have also studied the higher moments of the intensity $|\Psi|^2$ which are again determined by the hypothesis of Ψ being Gaussian distributed. One obtains as a theoretical expectation

$$\overline{\Psi^{2n}} = \int_{-\infty}^{\infty} \Psi^{2n} P(\Psi)\, \mathrm{d}\Psi = \frac{(2\sigma^2)^n}{\sqrt{\pi}}\, \Gamma(n + \tfrac{1}{2})\,. \tag{49}$$

We have compared the moments of intensity of the eigenstates with this theoretical prediction and found rough agreement, being aware of the fact that with increasing moment n ever finer details of the shape of the distribution are measured.

This Gaussian behaviour, which was expected in the limit $p \to \infty$, shows clearly up already at energies $E = 2000$ corresponding to $p \simeq 45$, which seems to be a somewhat low value. (Already at $E \simeq 200$ our earlier results [6] indicated a Gaussian behaviour.) However, the central limit theorem gives no clue about how fast the convergence towards the Gaussian distribution takes place, but our numerical results indicate a very fast convergence.

Table 2
The significance levels $\mathcal{P}$ of the cumulative amplitude distribution $I(\Psi)$ according to the Kolmogorov–Smirnov test with respect to the suggested Gaussian distribution are listed together with the skewness and the kurtosis.

E_n	$\mathcal{P}$ for $I(\Psi)$	Skewness	Skewness in standard deviations	Kurtosis	Kurtosis in standard deviations
2,000.695	93.8%	−0.0043	−0.249	−0.0747	−2.156
2,003.117	87.7%	0.0369	2.131	−0.1261	−3.639
2,005.110	35.6%	−0.0215	−1.241	−0.0968	−2.794
2,007.536	43.2%	−0.0154	−0.889	−0.1051	−3.034
2,009.041	72.4%	−0.0588	−3.392	0.0692	1.999
10,001.092	27.9%	−0.0192	−1.107	−0.0081	−0.235
10,003.405	70.0%	0.0143	0.826	0.0489	1.413
10,005.463	27.1%	−0.0154	−0.889	−0.0165	−0.477
10,006.061	72.7%	0.0207	1.195	−0.0139	−0.402
10,008.095	80.1%	−0.0084	−0.482	0.0028	0.081
10,011.254	25.8%	−0.0296	−1.706	−0.0769	−2.220
10,013.180	31.9%	0.0286	1.651	−0.0555	−1.603
10,013.697	90.6%	0.0399	2.302	−0.0449	−1.297
10,015.617	84.3%	−0.0089	−0.512	−0.0387	−1.119
10,016.972	29.6%	−0.0205	−1.183	−0.0505	−1.457
10,019.897	65.1%	−0.0088	−0.511	−0.0283	−0.817
20,001.170	42.1%	0.0083	0.477	−0.0099	−0.287
20,004.057	41.7%	−0.0046	−0.264	0.0905	2.611
20,004.915	99.9%	−0.0022	−0.132	0.0333	0.961
20,007.327	79.7%	0.0008	0.044	−0.0553	−1.596
20,008.391	68.8%	−0.0430	−2.485	0.0502	1.449
20,009.745	31.5%	0.0021	0.126	0.1059	3.058

5. Correlations in the wavefunctions

The autocorrelation function $C(\boldsymbol{q}, \boldsymbol{\tau})$ is defined as

$$C(\boldsymbol{q}, \boldsymbol{\tau}) = \frac{1}{\Pi(\boldsymbol{q})} \langle \Psi(\boldsymbol{q} - \tfrac{1}{2}\boldsymbol{\tau}) \Psi^*(\boldsymbol{q} + \tfrac{1}{2}\boldsymbol{\tau}) \rangle , \quad (50)$$

where $\boldsymbol{\tau}$ defines the distance and direction from the point $\boldsymbol{q}$ for which the autocorrelation is computed. The bracket $\langle\,\rangle$ denotes a local average over sufficiently many de Broglie wavelengths λ_B, and $\Pi(\boldsymbol{q})$ denotes the local average of the intensity

$$\Pi(\boldsymbol{q}) = \langle |\Psi(\boldsymbol{q})|^2 \rangle . \quad (51)$$

This autocorrelation function $C(\boldsymbol{q}, \boldsymbol{\tau})$ stands on a somewhat firmer theoretical ground than the prediction about the amplitude distribution. In [14] Berry derived $C(\boldsymbol{q}, \boldsymbol{\tau})$ for ergodic and integrable systems from the assumption that the Wigner function is semiclassically concentrated like a δ-function on the classically allowed phase space. For ergodic systems with N degrees of freedom, the semiclassical eigenfunction hypothesis (1) is inserted in the inverse Wigner transform

$$\Psi(\boldsymbol{q} - \tfrac{1}{2}\boldsymbol{\tau})\, \Psi^*(\boldsymbol{q} + \tfrac{1}{2}\boldsymbol{\tau}) = \int \mathrm{d}^N p\, W(\boldsymbol{q}, \boldsymbol{p})\, \mathrm{e}^{\mathrm{i}\boldsymbol{p}\boldsymbol{\tau}/\hbar} . \quad (52)$$

This approximation yields together with the definition (50)

$$C(\boldsymbol{q}, \boldsymbol{\tau}) = J_0(p\tau) , \quad p := |\boldsymbol{p}| \text{ and } \tau := |\boldsymbol{\tau}| \quad (53)$$

for $N = 2$ degrees of freedom where J_0 is the

Bessel function. (The general result is given in ref. [14].) For ergodic billiard systems ($V(q) = 0$ inside the domain) one expects thus an isotropic autocorrelation function if the contributions of the orbits in eq. (2) can be semiclassically neglected. In the integrable case the Wigner function is concentrated on the N-tori leading to an anisotropic system-dependent autocorrelation function.

The numerical studies carried out in the case of the stadium billiard in the range of the 600th eigenstate seem to indicate that the prediction (53) is not fulfilled, and the expected isotropy could not be found [30]. It thus seems that the orbit contributions in (2) cannot be neglected even at such highly excited states.

We have studied the autocorrelation function in the case of the wavefunctions of the hyperbolic octagon. There arises a small technical difficulty caused by the fact that it is not possible to single out a parallel to a given geodesic with respect to the hyperbolic metric (3). However, this is necessary for the local averaging required by the definition (50). To carry out the averaging one must obtain pairs of random points z_1, z_2 in the neighbourhood of "$z - \frac{1}{2}\tau$" and "$z + \frac{1}{2}\tau$" which have the same hyperbolic distance $\tau = d(z_1, z_2)$. This can be achieved by the following procedure. At first one chooses a boost b which transforms the origin $z = 0$ to some point $b(0)$ at which the autocorrelation function should be evaluated (see eq. (5)). Then one generates by a random number generator a set of matrices b^r which shift the origin to points $\hat{z}$ such that the $\hat{z}$'s are uniformly distributed in a disc of hyperbolic radius δ centred at the origin $z = 0$. This δ determines the averaging range which should cover several de Broglie wavelengths λ_B. For a given hyperbolic distance τ the two points at $z_\pm := \pm \tanh(\frac{1}{4}\tau)$ obey $d(z_-, z_+) = \tau$. With these two points one can obtain the desired set of pairs of random points by the prescription $z_1 := b(b^r(z_-))$ and $z_2 := b(b^r(z_+))$ because the transformations are conformal. In this way we generated 500 pairs of points whose connecting geodesics are parallel and have a common distance τ.

In figs. 14–17 we present the results which are obtained for the eigenstates at $E = 10\,001.092$ and $E = 10\,003.405$. To emphasize the role of the size of the averaging disc, we display the results in dependence of the radius δ in units of the de Broglie wavelength λ_B. The computations cover the range from λ_B to $26\lambda_B$. In figs. 15 and 17 we have subtracted the theoretical prediction (53) and it is seen that the prediction is not fulfilled very well even at the largest averaging radius $\delta = 26\lambda_B$. Furthermore, the error does not seem to decline appreciably with increasing radius δ in both cases. Thus one must conclude that the wavefunctions display on such scales much more structure than is compatible with the semiclassical eigenfunction hypothesis (1) from which the prediction (53) derives. This is consistent with the observed structure of the wavefunctions already displayed in figs. 1–4, which clearly show a non-isotropic behaviour up to scales of roughly 20 de Broglie wavelengths. This non-universal This non-universal behaviour is also reflected in a z-dependence of the correlation function.

However this negative result does not exclude the possibility that the prediction (53) describes the autocorrelation correctly on much larger averaging domains. To scrutinize that possibility, we turn now to another version of a correlation measure, i.e. to the path-correlation function as it was proposed by Shapiro and Goelman [29]. The path-correlation function

$$C_{\mathscr{C}}(\tau) = \frac{1}{L} \int_{\mathscr{C}} \mathrm{d}q\, \Psi^*(q)\, \Psi(q + \tau) \tag{54}$$

averages the correlation over a given path $\mathscr{C}$ of length L which is "self-avoiding space filling" [29]. Consider as the path $\mathscr{C}$ a semicircle with radius ρ centred at the origin of the Poincaré disc $\mathscr{D}$, i.e.

$$C(\phi) = \frac{1}{\pi} \int_0^\pi \mathrm{d}\theta\, \Psi^*(\rho, \theta)\, \Psi(\rho, \theta + \phi)\,, \tag{55}$$

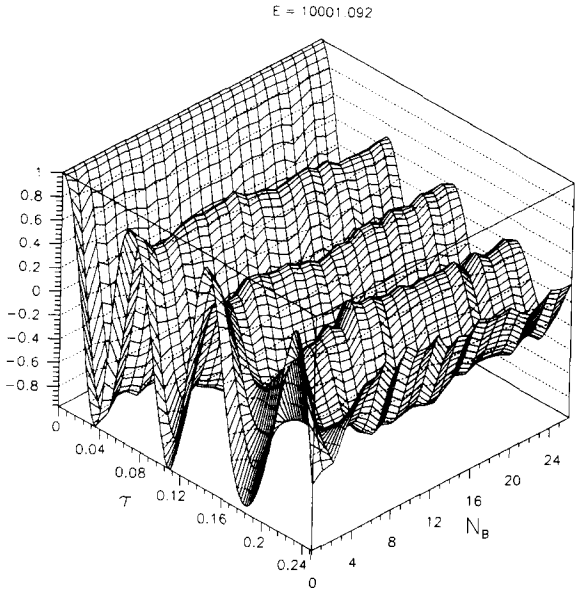

Fig. 14. The autocorrelation $C(q, \tau)$ is shown for the eigenstate at $E = 10\,001.092$ in dependence of τ and of the number N_B of de Broglie wavelengths λ_B over which the averaging has been carried out.

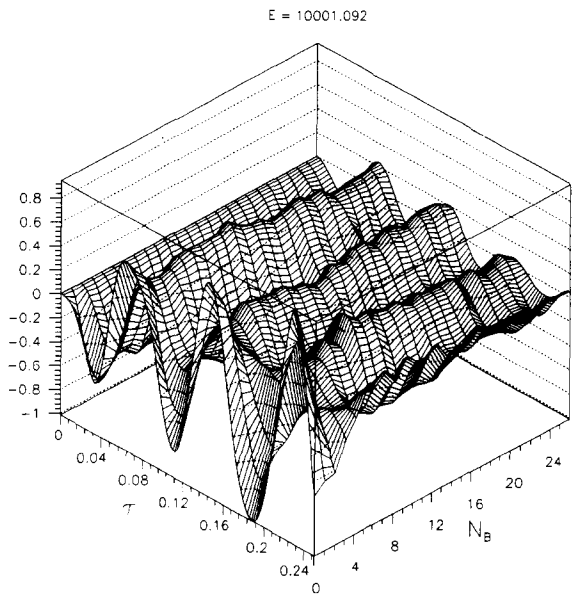

Fig. 15. The theoretical prediction $J_0(p\tau)$ has been subtracted from the autocorrelation $C(q, \tau)$ which is shown in fig. 14.

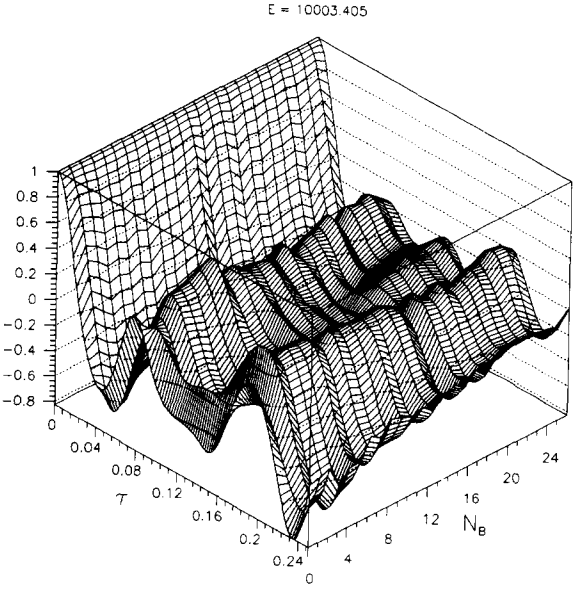

Fig. 16. The autocorrelation $C(q, \tau)$ is shown for the eigenstate at $E = 10\,003.405$ in dependence of τ and of the number N_B of de Broglie wavelengths λ_B over which the averaging has been carried out.

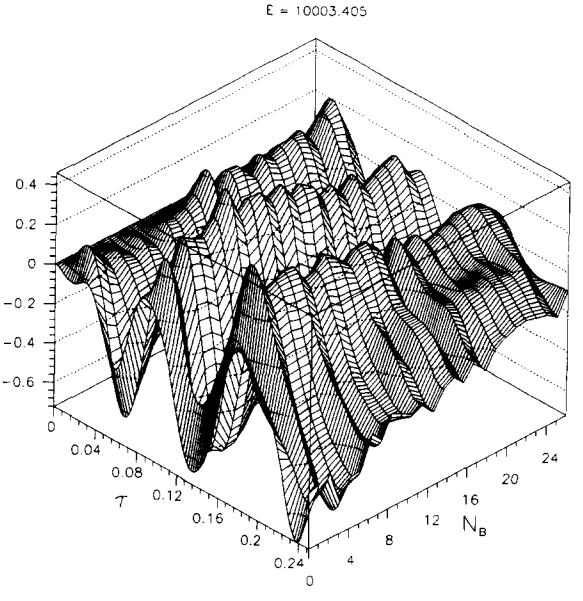

Fig. 17. The theoretical prediction $J_0(p\tau)$ has been subtracted from the autocorrelation $C(q, \tau)$ which is shown in fig. 16.

where the angle ϕ determines the hyperbolic distance $\tau = d(z_1, z_2)$ of the two points $z_1 = \tanh(\rho/2)\,\mathrm{e}^{\mathrm{i}\theta}$ and $z_2 = \tanh(\rho/2)\,\mathrm{e}^{\mathrm{i}(\theta+\phi)}$, which yields with (13)

$$\cosh\tau = \cosh^2\rho - \sinh^2\rho\cos\phi\,. \tag{56}$$

Inserting the circular-wave expansion (25) in eq. (55), one obtains

$$C(\phi) = \tfrac{1}{4}A_0^2\,F_0^2(s,\rho) + \frac{1}{2}\sum_{n=1}^{\infty} A_n^2\cos(2n\phi)\,F_{2n}^2(s,\rho)\,, \tag{57}$$

with $A_n^2 = a_{2n-1}^2 + a_{2n}^2$ and $A_0 = a_0$ being the coefficients of the expansion (31). Here the sum runs only over the even indices of $F_m(s,\rho)$ which is due to the positive parity which was assumed. In the case of negative parity, only the odd indices would appear. Let us assume for a moment that the indices are not restricted, i.e. consider

$$\tilde{C}(\phi) = \frac{1}{4}\Big(A_0^2F_0^2(s,\rho) + 2\sum_{n=1}^{\infty} A_n^2\cos(n\phi)\,F_n^2(s,\rho)\Big)\,. \tag{58}$$

The coefficients A_n are random numbers (see section 3), but one can approximate the series by replacing the A_n^2's by their mean $\overline{A^2} > 0$:

$$\tilde{C}(\phi) \simeq \frac{\overline{A^2}}{4}\Big(F_0^2(s,\rho) + 2\sum_{n=1}^{\infty}\cos(n\phi)\,F_n^2(s,\rho)\Big)\,. \tag{59}$$

From the addition theorem of the Legendre functions (see Appendix G in ref. [21]) one derives the relation

$$F_0^2(s,\rho) + 2\sum_{n=1}^{\infty}\cos(n\phi)\,F_n^2(s,\rho) = F_0(s,\tau) = P_{-s}(\cosh\tau)\,, \tag{60}$$

where τ is given by eq. (56). Thus one arrives at the simple expression

$$\tilde{C}(\phi) \simeq \tfrac{1}{4}\overline{A^2}P_{-s}(\cosh\tau)\,. \tag{61}$$

In the semiclassical limit one recovers the prediction (53) because of

$$\lim_{\nu\to\infty} P_\nu(\cosh(z/\nu)) = I_0(z)\,, \tag{62}$$

with $z = \mathrm{i}p\tau$ and $I_0(\mathrm{i}p\tau) = J_0(p\tau)$. Thus one ends up with

$$\tilde{C}(\phi) \simeq \tfrac{1}{4}\overline{A^2}\,J_0(p\tau)\,. \tag{63}$$

This corresponds exactly to the prediction (53) since (53) holds with respect to the definition (50) where the local average of the intensity $\Pi(\boldsymbol{q}) = C(0) = \overline{A^2}/4$ has been divided out.

The above derivation has been carried out under the assumption that all indices in the sum over F_n^2 contribute. If that does not happen as in the expansions (25) and (57), one can eliminate the wrong terms by the recursion formula of the Legendre functions of the type $F_n = aF_{n-1} + bF_{n+1}$. Because of the square one has mixed terms $F_{n-1}F_{n+1}$ in addition. These additional terms only vanish if one averages in the τ-direction, i.e. evaluates $C(\phi)$ on an annulus of finite width. Thus we have recovered the prediction (53) from the fact that the eigenstates are not localized with respect to the circular-wave basis. This justifies the replacement of the A_n^2's by their mean $\overline{A^2}$, since there are infinitely many coefficients A_n of the same order with a common variance (see section 3). In addition, the accuracy of this replacement depends on the momentum p and the hyperbolic radius ρ of the semicircle, because the effective contribution of the A_n's is governed by the magnitude of the function $F_n(s,\rho)$. As already stated, there are approximately $N \simeq p\,\sinh\rho$ contributing circular waves. The above replacement thus requires $N \to \infty$, i.e. the semiclassical limit $p \to \infty$.

In fig. 18 the path-correlation function (54) is shown in comparison with the theoretical expectations (53) and (61), where in the latter case the local average of the intensity has been divided out. The Legendre function occurring in eq. (61) is already at $E \simeq 2000$ so well approximated by the Bessel function J_0 that no difference is visible in this figure. It is seen that the path-correlation matches the prediction quite well. However, there are nevertheless deviations showing clearly the error which is introduced by replacing the true coefficients A_n^2 by their mean $\overline{A^2}$. To emphasize the role played by the size of the averaging domain, note that the averaging takes place over a large number of de Broglie wavelengths λ_B given by

$$\frac{L}{\lambda_B} = \frac{p \sinh \rho}{2} = \frac{pr}{1-r^2}\,,$$
$$r := \tanh \tfrac{1}{2}\rho\,. \tag{64}$$

In figs. 18a and 18b, which correspond to eigenstates at $E \simeq 2000$, the averaging takes place over $\sim 414\lambda_B$, and in figs. 18c and 18d, i.e. at $E \simeq 10\,000$, one gets $\sim 927\lambda_B$, where $r = 0.9475$ has been used in all cases.

At last we would like to turn briefly to the cross-correlation function which measures the

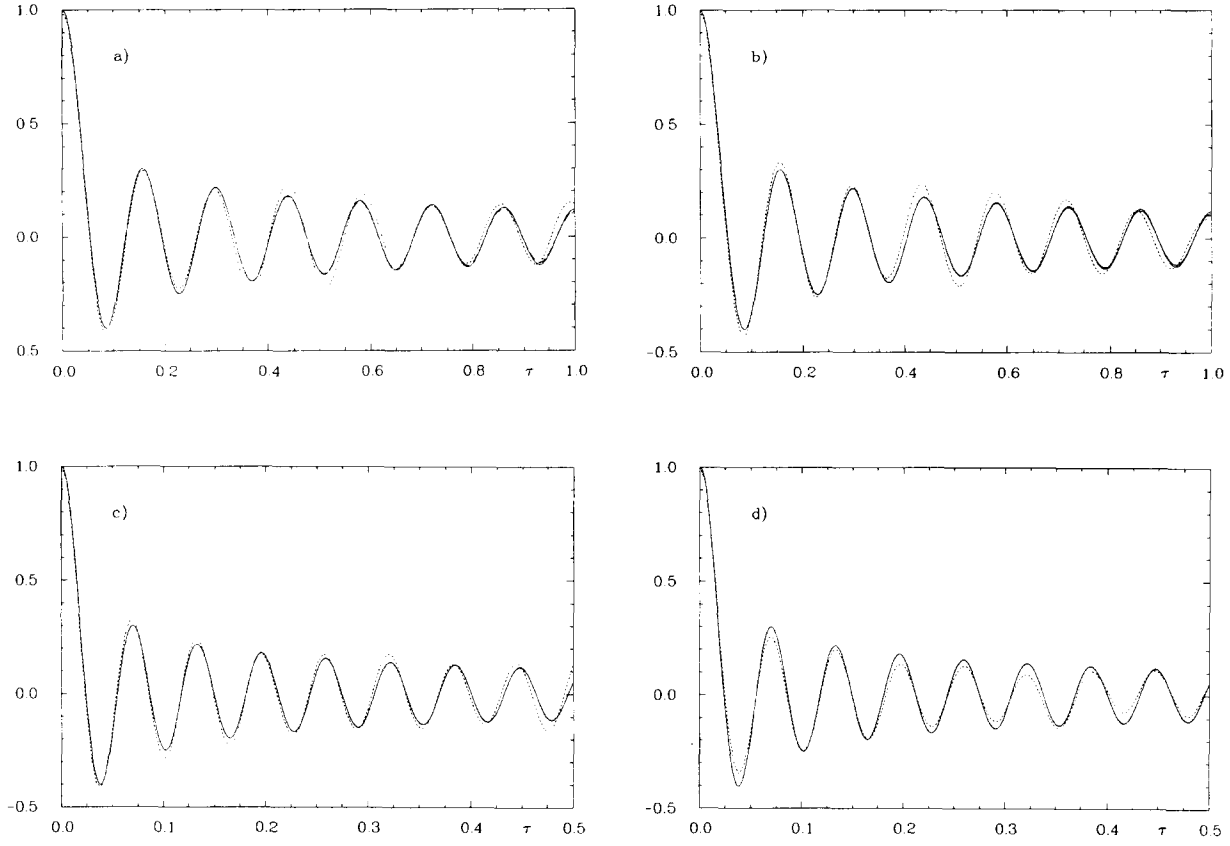

Fig. 18. The path-correlation function (54) is displayed as a dotted curve for the same four eigenstates as in the preceding figures. The chosen path is a semicircle with Euclidean radius $r = 0.9475$ in the Poincaré disc. The theoretical predictions (53) as well as (61) are shown as full curves where in the latter the local average of the intensity $\Pi(q) = C(0) = \overline{A^2}/4$ has been divided out. Both curves are lying so closely together that they are not resolved in this figure.

correlations between different eigenstates. This is an important measure in the study of the characteristic properties of the time evolution of a given initial state of a chaotic system (see e.g. [32]). The general assumption is that the eigenstates are not correlated among each other and thus the cross-correlation should vanish for chaotic systems. We have checked this for the eigenstates at $E \simeq 10\,000$ and have found indeed very small cross-correlations compatible with this assumption. This result can also be derived from the path-correlation function. If one inserts in (54) the circular-wave expansions (25) corresponding to two different states, one ends up with coefficients of the form $\hat{A}_n := a_{2n-1}a'_{2n-1} + a_{2n}a'_{2n}$ instead of A_n^2, where a and a' belong to the two different states. If one assumes that the coefficients of different states are not correlated, then it follows that the mean of $\hat{A}_n$ is zero. From eq. (61) one thus obtains a vanishing cross-correlation function.

6. Summary

In this paper we have studied the statistical properties of highly excited eigenstates of a strongly chaotic system (K-system). The system considered consists classically of a point particle sliding freely on a compact Riemann surface of constant negative curvature of genus $g = 2$, i.e. on a hyperbolic octagon. The quantum mechanics is governed by the Schrödinger equation (4) subject to periodic boundary conditions. All eigenstates up to $E = 2050$ and in the energy intervals $[10\,000,\ 10\,020]$ and $[20\,000, 20\,010]$ with positive parity have been computed by the boundary-element method for a generic asymmetric hyperbolic octagon. Within this parity class, the eigenstates at $E \simeq 20\,000$ are lying 10 000 states above the ground state and are thus probing the semiclassical limit.

The eigenstates have been expanded in the circular-wave basis (25), and the expansion coefficients a_n have been studied with respect to their statistical properties. It has been numerically shown that the eigenstates are not localized with respect to this basis and that the coefficients a_n are Gaussian distributed. The correlation function $C(j)$, defined in (35), shows no correlations among the a_n's which can thus be considered as Gaussian pseudo-random numbers. In addition, the isotropy of the circular waves has been studied by the expansion (31) revealing indeed isotropy and thus, as expected for a strongly chaotic system, that no direction is singled out. Hence, these eigenstates are as random as it is conceivable.

The amplitude distribution $P(\Psi)$ has been investigated and compared with the hypothesis that it should reveal a Gaussian distribution of the amplitudes Ψ in the case of chaotic systems. For the integrable case it is expected that the invariant tori in phase space lead to distinct system-dependent amplitude distributions being non-Gaussian. By computing the amplitude distributions of the circular waves combined with the numerical fact that the coefficients a_n are Gaussian random variables, it could be shown using the central limit theorem that the amplitude distribution $P(\Psi)$ indeed converges towards a Gaussian in the semiclassical limit. This prediction, which is in agreement with the common expectations, could be numerically confirmed in the case of all eigenstates studied by us. Furthermore, higher moments of the distribution $P(\Psi)$ have been considered, while the skewness and the kurtosis have been discussed in more detail. Even these very sensitive measures testing the tails and the shape of $P(\Psi)$ are in agreement with a Gaussian distribution.

Finally, the autocorrelation function $C(\boldsymbol{q}, \boldsymbol{\tau})$ was studied in comparison with the theoretical expectation (53) based on the crudest possible approximation of the Wigner function, i.e. a δ-function concentrated on the energy surface in phase space. The expectation (53) presupposes that structures in the eigenstates occur only on small scales which are averaged out within the

local average $\langle\rangle$. Our numerical comparisons show, however, that the eigenstates display much more structure even if the averaging is carried out over domains containing as many as 50 de Broglie wavelengths λ_B. Even worse, as seen in figs. 14–17, the error does not seem to decline appreciably with a growing averaging domain. A similar result was obtained in the case of the stadium billiard [30] where also too much structure was observed. Thus we were led to study the behavior in the limit of much larger averaging domains, where the path-correlation function (54) is more appropriate. Furthermore it allows a simple analytical computation of the correlation function in terms of the circular-wave expansion coefficients. It is shown that in the semiclassical limit $p \to \infty$ the non-localization within this basis leads to the prediction (53). Despite the averaging over nearly 1000 de Broglie wavelengths λ_B, small deviations from (53) are observed (see fig. 18), and one might wonder whether such domains should still be called "local". We thus conclude that the expectation (53) describes the statistical properties of our eigenstates only on exceedingly large averaging domains. The needed domains are so extended that the "decorations" on the energy surface in the Wigner function are completely washed out which is mimicked by our replacement of the true coefficients A_n^2 by their mean. Thus a better theory is required for the description of the correlations of the eigenstates incorporating individual properties of the eigenstates as it is provided by the orbit theory developed in ref. [19]. Unfortunately, the computational problems due to the summation over an exponentially increasing number of orbit contributions is a serious obstacle.

Acknowledgement

We would like to thank the Deutsche Forschungsgemeinschaft for financial support and the HLRZ at Jülich for the access to the CRAY Y-MP 832 computer.

References

[1] M.L. Mehta, Random Matrices and the Statistical Theory of Energy Levels (Academic Press, New York, 1967) and new revised and enlarged edition, 1990.
[2] O. Bohigas and H.A. Weidenmüller, Ann. Rev. Nucl. Part. Sci. 38 (1988) 421.
[3] O. Bohigas, Random Matrix Theories and Chaotic Dynamics, in: Proc. 1989 Les Houches School on Chaos and Quantum Physics, M.-J. Giannoni, A. Voros and J. Zinn-Justin, eds. (Elsevier, Amsterdam, 1991).
[4] M.C. Gutzwiller, Chaos in Classical and Quantum Mechanics (Springer, New York, 1990).
[5] F. Haake, Quantum Signatures of Chaos (Springer, Berlin, 1991).
[6] R. Aurich and F. Steiner, Physica D 43 (1990) 155.
[7] E.P. Wigner, Phys. Rev. 40 (1932) 749.
[8] T.A. Brody, J. Flores, J.B. French, P.A. Mello, A. Pandey and S.S.M. Wong, Rev. Mod. Phys. 53 (1981) 385.
[9] F. Haake and K. Zyczkowski, Phys. Rev. A 42 (1990) 1013.
[10] F.M. Izrailev, Phys. Rep. 196 (1990) 299.
[11] E.J. Heller, Phys. Rev. Lett. 53 (1984) 1515; Springer Lecture Notes in Physics, Vol. 263 (1986) p. 162.
[12] A.I. Shnirelman, Usp. Mat. Nauk. 29 (1974) 181.
[13] A. Voros, Ann. Inst. H. Poincaré 24 A (1976) 31.
[14] M.V. Berry, J. Phys. A 10 (1977) 2083; Phil. Trans. Roy. Soc. A 287 (1977) 237; Semiclassical Mechanics of Regular and Irregular Motion, in: Les Houches Summer School, Sect. XXXVI, G. Iooss, R.H.G. Helleman and R. Stora, eds. (North-Holland, Amsterdam, 1983) p. 171.
[15] S. Zelditch, Duke Math. J. 55 (1987) 919.
[16] Y. Colin de Verdière, Commun. Math. Phys. 102 (1985) 497.
[17] E.B. Bogomolny, Physica D 31 (1988) 169.
[18] M.V. Berry, Proc. R. Soc. London A 423 (1989) 219.
[19] R. Aurich and F. Steiner, Physica D 48 (1991) 445.
[20] I.M. Gelfand and S.V. Fomin, Transl. Amer. Math. Soc. 2 No. 1 (1955) 49.
[21] N.L. Balazs and A. Voros, Phys. Rep. 143 (1986) 109.
[22] R. Aurich and F. Steiner, Physica D 39 (1989) 169.
[23] C. Grosche and F. Steiner, Ann. Phys. (NY) 182 (1988) 120.
[24] W. Magnus, F. Oberhettinger and R.P. Soni, Formulas and Theorems for the Special Functions of Mathematical Physics (Springer, Berlin, 1966), third edition.
[25] R. Aurich and F. Steiner, Phys. Rev. A 45 (1992) 583.
[26] M. Kuś, J. Mostowski and F. Haake, J. Phys. A 21 (1988) L1073.

[27] Y. Alhassid and M. Feingold, Phys. Rev. A 39 (1989) 374.
[28] R. von Mises, Mathematical Theory of Probability and Statistics (Academic Press, New York, 1964).
[29] M. Shapiro and G. Goelman, Phys. Rev. Lett. 53 (1984) 1714.
[30] S.W. McDonald and A.N. Kaufmann, Phys. Rev. A 37 (1988) 3067.
[31] Bateman Manuscript Project, Higher Transcendental Functions, Vol. I, A. Erdélyi, ed. (McGraw-Hill, New York, 1953).
[32] M. Shapiro, J. Ronkin and P. Brumer, Chem. Phys. Lett. 148 (1988) 177.